

# The *Gaia*-ESO Survey: Calibration strategy<sup>★,★★</sup>

E. Pancino<sup>1,2</sup>, C. Lardo<sup>3</sup>, G. Altavilla<sup>4</sup>, S. Marinoni<sup>5,2</sup>, S. Ragaini<sup>4</sup>, G. Cocozza<sup>4</sup>, M. Bellazzini<sup>4</sup>, E. Sabbi<sup>6</sup>, M. Zoccali<sup>7,8</sup>, P. Donati<sup>4,9</sup>, U. Heiter<sup>10</sup>, S. E. Koposov<sup>11</sup>, R. Blomme<sup>12</sup>, T. Morel<sup>13</sup>, S. Simon-Díaz<sup>14,15</sup>, A. Lobel<sup>12</sup>, C. Soubiran<sup>16</sup>, J. Montalbán<sup>17,27</sup>, M. Valentini<sup>18</sup>, A. R. Casey<sup>11</sup>, S. Blanco-Cuaresma<sup>19</sup>, P. Jofré<sup>11,20</sup>, C. C. Worley<sup>11</sup>, L. Magrini<sup>1</sup>, A. Hourihane<sup>11</sup>, P. François<sup>21,39</sup>, S. Feltzing<sup>22</sup>, G. Gilmore<sup>11</sup>, S. Randich<sup>1</sup>, M. Asplund<sup>23</sup>, P. Bonifacio<sup>21</sup>, J. E. Drew<sup>24</sup>, R. D. Jeffries<sup>25</sup>, G. Micela<sup>26</sup>, A. Vallenari<sup>27</sup>, E. J. Alfaro<sup>28</sup>, C. Allende Prieto<sup>14,15</sup>, C. Babusiaux<sup>21</sup>, T. Bensby<sup>22</sup>, A. Bragaglia<sup>4</sup>, E. Flaccomio<sup>26</sup>, N. Hambly<sup>29</sup>, A. J. Korn<sup>10</sup>, A. C. Lanzafame<sup>30,34</sup>, R. Smiljanic<sup>31</sup>, S. Van Eck<sup>32</sup>, N. A. Walton<sup>11</sup>, A. Bayo<sup>33</sup>, G. Carraro<sup>17</sup>, M. T. Costado<sup>28</sup>, F. Damiani<sup>26</sup>, B. Edvardsson<sup>10</sup>, E. Franciosini<sup>1</sup>, A. Frasca<sup>34</sup>, J. Lewis<sup>11</sup>, L. Monaco<sup>35</sup>, L. Morbidelli<sup>1</sup>, L. Prisinzano<sup>26</sup>, G. G. Sacco<sup>1</sup>, L. Sbordone<sup>8,7,36</sup>, S. G. Sousa<sup>37</sup>, S. Zaggia<sup>27</sup>, and A. Koch<sup>38</sup>

(Affiliations can be found after the references)

Received 1 August 2016 / Accepted 20 October 2016

## ABSTRACT

The *Gaia*-ESO survey (GES) is now in its fifth and last year of observations and has produced tens of thousands of high-quality spectra of stars in all Milky Way components. This paper presents the strategy behind the selection of astrophysical calibration targets, ensuring that all GES results on radial velocities, atmospheric parameters, and chemical abundance ratios will be both internally consistent and easily comparable with other literature results, especially from other large spectroscopic surveys and from *Gaia*. The calibration of GES is particularly delicate because of (i) the large space of parameters covered by its targets, ranging from dwarfs to giants, from O to M stars; these targets have a large wide of metallicities and also include fast rotators, emission line objects, and stars affected by veiling; (ii) the variety of observing setups, with different wavelength ranges and resolution; and (iii) the choice of analyzing the data with many different state-of-the-art methods, each stronger in a different region of the parameter space, which ensures a better understanding of systematic uncertainties. An overview of the GES calibration and homogenization strategy is also given, along with some examples of the usage and results of calibrators in GES iDR4, which is the fourth internal GES data release and will form the basis of the next GES public data release. The agreement between GES iDR4 recommended values and reference values for the calibrating objects are very satisfactory. The average offsets and spreads are generally compatible with the GES measurement errors, which in iDR4 data already meet the requirements set by the main GES scientific goals.

**Key words.** surveys – Galaxy: general – stars: abundances – techniques: spectroscopic – techniques: radial velocities

## 1. Introduction

The detailed study of the Milky Way (MW) as a galaxy has emerged as a central field in modern astrophysics and is currently attracting much attention, not the least thanks to the launch of the *Gaia* ESA space mission in December 2013 (Gaia Collaboration 2016a; Gaia Collaboration 2016b; Lindegren & Perryman 1996; Mignard 2005; de Bruijne 2012). For in-depth studies of the properties of the stellar populations in the MW, high-multiplex spectroscopy of sufficient resolution is required to obtain radial velocities (RV), stellar astrophysical parameters (AP), and elemental abundances for large numbers of stars (Freeman & Bland-Hawthorn 2002; Bland-Hawthorn et al. 2010). Several new instruments have been designed around this idea (including HERMES, 4MOST, and WEAVE; Barden et al. 2010; de Jong et al. 2014; Balcells et al. 2010), and several spectroscopic surveys are ongoing or planned with this goal in mind (for example, RAVE, APOGEE, GALAH, and LEGUE; Kordopatis et al. 2013; Majewski et al. 2016; De Silva et al. 2015; Newberg et al. 2012). All these surveys will study millions of stars, but they

will adopt different selection criteria, instrumental setups, and data analysis methods.

The *Gaia*-ESO public spectroscopic survey (GES, Gilmore et al. 2012; Randich et al. 2013) started operations at the end of 2011, with the goal of exploring all components of the MW in a complementary way to *Gaia*. GES uses the FLAMES optical spectrograph (Pasquini et al. 2000) at the European Southern Observatory (ESO) Very Large Telescope (VLT), in Medusa combined mode, where 6 to 8 fibers are used by UVES with a resolution of  $R = \lambda/\Delta\lambda \simeq 47\,000$ , and 132 fibers are used by GIRAFFE, with  $R \simeq 16\,000$ – $25\,000$ , depending on the wavelength range chosen (see Table 1 for a list of the GES observing setups used). GES is measuring RVs and derives APs and chemical abundances of several elements for  $\sim 10^5$  stars, focussing on relatively faint stars (mainly  $V > 16$  mag), for which *Gaia* will not be able to provide accurate RVs and abundances. GES data have their own outstanding scientific and legacy value, but together with the *Gaia* data, they will provide extremely detailed 6D space information (position, distance, and 3D motions), combined with astrophysical information, for a representative sample of MW stars.

Stellar spectroscopic surveys require specific calibrators to allow for meaningful comparisons with other literature studies and spectroscopic surveys, but also for internal homogenization purposes. GES has chosen to invest a significant effort on calibrations because of the great variety of stellar targets, and

\* Based on data products from observations made with ESO Telescopes at the La Silla Paranal Observatory under programme IDs 188.B-3002 and 193.B-0936.

\*\* Full Table 2 is only available at the CDS via anonymous ftp to [cdsarc.u-strasbg.fr](http://cdsarc.u-strasbg.fr) (130.79.128.5) or via <http://cdsarc.u-strasbg.fr/viz-bin/qcat?J/A+A/598/A5>

**Table 1.** FLAMES instrumental setups used in the *Gaia*-ESO Survey, with the number of individual stars analyzed in iDR4 for each setup.

| Instrument | Setup                | $\lambda_{\min}$<br>(Å) | $\lambda_{\max}$<br>(Å) | $R$<br>( $\lambda/\Delta\lambda$ ) | iDR4   |
|------------|----------------------|-------------------------|-------------------------|------------------------------------|--------|
| UVES       | 520 <sup>a,d</sup>   | 4140                    | 6210                    | 47 000                             | 337    |
| UVES       | 580 <sup>b,d</sup>   | 4760                    | 6840                    | 47 000                             | 3281   |
| UVES       | 860 <sup>c</sup>     | 6600                    | 10 600                  | 47 000                             | –      |
| GIRAFFE    | HR3 <sup>a,d</sup>   | 4033                    | 4201                    | 24 800                             | 822    |
| GIRAFFE    | HR4 <sup>a,e</sup>   | 4188                    | 4297                    | 24 000                             | –      |
| GIRAFFE    | HR5A <sup>a,d</sup>  | 4340                    | 4587                    | 18 470                             | 823    |
| GIRAFFE    | HR6 <sup>a,d</sup>   | 4538                    | 4759                    | 20 350                             | 806    |
| GIRAFFE    | HR9B <sup>d</sup>    | 5143                    | 5356                    | 25 900                             | 2243   |
| GIRAFFE    | HR10 <sup>f</sup>    | 5339                    | 5619                    | 19 800                             | 29 215 |
| GIRAFFE    | HR14A <sup>a,d</sup> | 6308                    | 6701                    | 17 740                             | 683    |
| GIRAFFE    | HR15N <sup>d</sup>   | 6470                    | 6790                    | 17 000                             | 19 431 |
| GIRAFFE    | HR21 <sup>f</sup>    | 8484                    | 9001                    | 16 200                             | 31 649 |

**Notes.** The official ESO setup data presented here refer to the period covered by GES iDR4 observations, i.e., before August 2014. <sup>(a)</sup> Mostly used for OBA stars (WG13). <sup>(b)</sup> Mostly used for FGK stars (WG10, WG11, WG12). <sup>(c)</sup> Used for benchmark stars (legacy value only, no analysis). <sup>(d)</sup> Used for OCs; HR09B is generally used for stars of type A, and hotter, while HR15N is used for stars of type F and cooler. <sup>(e)</sup> Not in iDR4, introduced only recently. <sup>(f)</sup> Used for MW field stars.

the consequent observational setups and analysis methods. Of course, the calibration objects do not serve only to assess the internal consistency, but also to allow for external comparisons with other large surveys and with *Gaia*. This will maximize their legacy value and provide a rich reference dataset for future inter-survey calibrations.

In this paper we describe the GES calibration needs, the calibrating targets selection and observation processes, and the various uses and purposes of the chosen calibrators in the framework of the GES data analysis. We use the GES iDR4 data<sup>1</sup> to illustrate how the calibrators are employed in GES, and with which results. The paper is organized as follows: in Sect. 2 we discuss the general basis and implementation of the GES calibration strategy; the following sections discuss various types of calibrators such as RV standards (Sect. 3), open and globular clusters (OC and GC, respectively, Sect. 5), benchmark stars (Sect. 4), and astroseismologic constraints (Sect. 6). In Sect. 7 we present our summary and conclusions.

## 2. GES calibration requirements and strategy

The broad scientific goal of GES is to survey all MW components, including the disk(s), the bulge, the halo, with special attention to the solar neighborhood, which will be studied by *Gaia* in extreme detail (Gilmore et al. 2012). GES includes OCs of all ages, excluding only those that are still embedded (Randich et al. 2013), to study their internal properties and evolution, and their role as tracers of the thin-disk population.

<sup>1</sup> GES iDR4 is the fourth internal data release, where a large part of the data obtained before the end of August 2014 were reanalyzed homogeneously, taking into account the lessons learned in the previous internal releases. GES iDR4 will also form the basis of the next GES public data release through the ESO Phase3 portal for public surveys, which is expected soon.

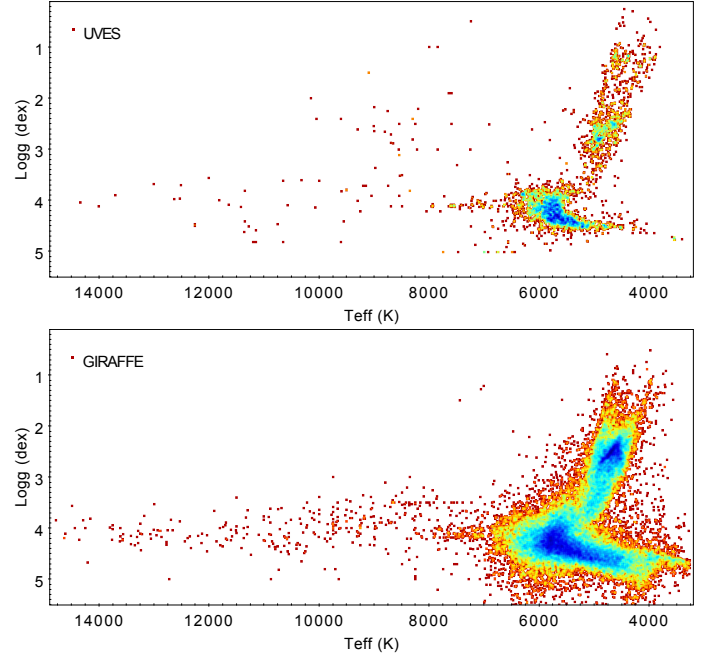


**Fig. 1.** Parameter coverage of GES iDR4 stars. The top panel shows stars observed with UVES and the bottom one with GIRAFFE. The color-scale refers to the density of points (red is low density while blue is high). A long tail of hot stars extending to  $T_{\text{eff}} > 14\,000$  K was cut for plot readability.

As a result, GES targets cover a wide range of properties, from dwarfs to giants, from O to M stars, and with a wide range of metallicities and abundance patterns. Figure 1 shows the parameter space coverage of the 54 530 iDR4 GES targets for which recommended parameters<sup>2</sup> were produced. The corresponding [Fe/H] distribution is presented in Fig. 2. As a first obvious requirement, GES calibrators must adequately cover this wide range of properties.

The analysis of the stellar spectra obtained by GES has been organized in a set of Working Groups (WGs). The characteristics of each WG are described in detail elsewhere, but we summarize them here briefly. WG10 deals with the GIRAFFE analysis of FGK stars (Recio-Blanco et al., in prep.), WG11 with the UVES analysis of FGK stars (Smiljanic et al. 2014), WG12 with the analysis of pre-MS and of cool stars (Lanzafame et al. 2015), and WG13 with the analysis of hot stars (Blomme et al., in prep.). Within each WG, almost all state-of-the-art methods, appropriate for different objects, are implemented and applied by various research groups, which are called *abundance analysis nodes*. They cover various methods, from full spectral synthesis to classical equivalent width (EW) techniques, and use a variety of abundance computation codes. Some are more suited to deal with specific stellar properties such as stellar rotation or veiling. Others were designed for accurate measurements of specific features, for example, lithium or the  $H_{\alpha}$  line. More details on the individual node abundance analysis methods can be found in the above cited papers that describe the WG analysis. This is a main strength of GES because it allows for method intercomparisons that are extremely instructive on the strengths, weaknesses, and applicability ranges of each method, and for a deep knowledge of systematic errors. However, this complexity of the data analysis

<sup>2</sup> Here and in the rest of the paper, the recommended values, APs, RVs, or abundances are the final values produced by GES after the whole homogenization procedure.

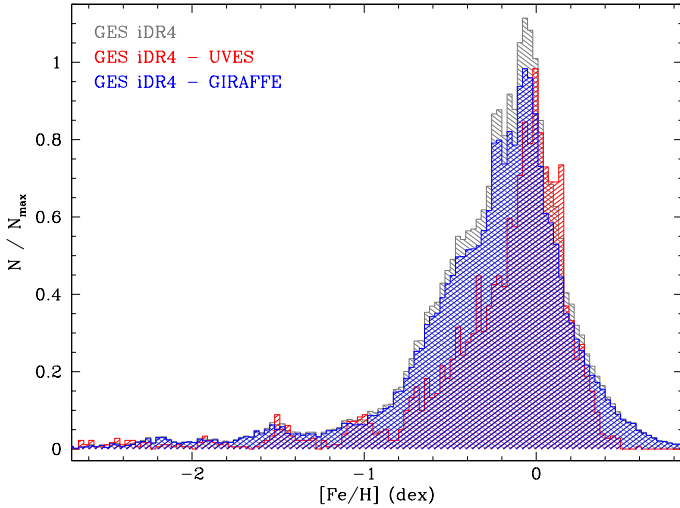


**Fig. 2.** Metallicity distribution of GES iDR4 targets as a whole (gray shaded histogram) and of the UVES (red shaded) and GIRAFFE (blue shaded) targets in iDR4. The histogram of the whole sample was normalized differently for clarity.

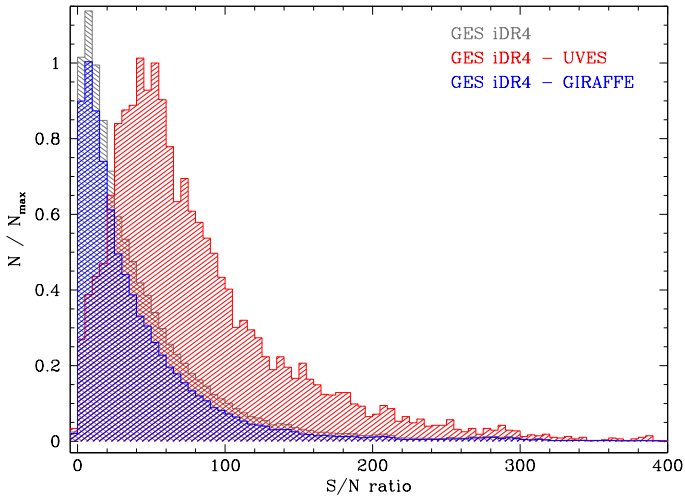


**Fig. 3.** Histogram of the S/N distribution for individual spectra in GES iDR4 (gray shaded histogram), and of UVES (red shaded) and GIRAFFE (blue shaded) individual spectra. The whole iDR4 sample was normalized differently for clarity.

places another strong requirement on the calibration strategy: that an adequate number of calibrating objects also needs to fall into those regions of the parameter space that are analyzed by more than one WG and node.

Finally, as a natural consequence of the great variety of science targets and methods, the observing strategy relies on several different observing setups that are appropriate for different types of objects and are summarized in Table 1. In addition, depending on the science goal (focus on RVs or on chemical abundances), a wide range of signal-to-noise ratios (S/N) were obtained, as shown in Fig. 3. This places another requirement on GES calibrations: an adequate number of (calibrating) objects need to be observed with more than one setup and with a range of S/N.

All the calibration requirements described above ensure that GES is both internally consistent with respect to the different methods, objects, and observational setups, and easily comparable with other literature results. Therefore, a good fraction of the calibrators need to be well-studied objects with reliable

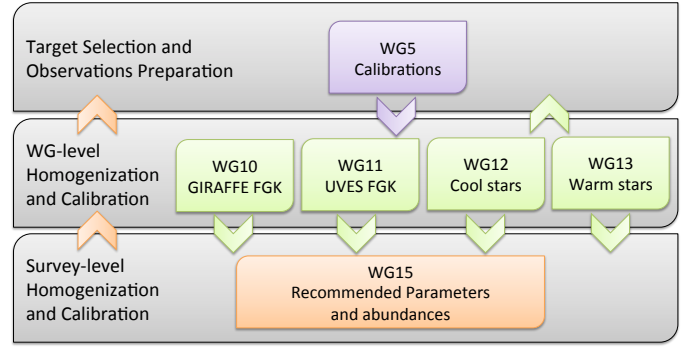


**Fig. 4.** Iterative GES calibration and homogenization process. Arrows mark the flow of information from target selection (described in this paper) to abundance analysis and production of recommended parameters and abundances. Between and during abundance analysis cycles, feedback is provided by the downstream layers, to refine the calibration observations and the analysis strategy. Only those WGs that make use of calibrators are indicated in this figure.

reference parameters and abundances. It is also desirable that some of the calibrators are observed by other large surveys as well to enhance the legacy value of GES. The ensemble of all the internal and external calibration procedures in GES is referred to as homogenization.

### 2.1. GES analysis workflow

GES data analysis proceeds in cycles, also called internal data releases (iDR). Within each cycle, the survey calibration and homogenization is organized in three logical layers, as illustrated in Fig. 4. The starting one, coordinated by WG5, takes care of selecting the appropriate calibrating objects and of preparing their observations, which is the main topic of the present paper. In a second layer, appropriate calibrators are used by the WGs to compare and combine the node-level APs and abundances into WG-level recommended parameters. Finally, at different stages in each cycle, WG15 performs a homogenization of the WG-level results to provide survey-level recommended RVs, APs, and chemical abundance ratios.

Internal consistency among abundance analysis nodes is facilitated as much as possible<sup>3</sup> by the use of a common set of atmospheric models (MARCS, see, Gustafsson et al. 2008), a common line list (Heiter et al. 2015a), and a common grid of synthetic spectra, based upon the grid by de Laverny et al. (2012). For the first processing cycles up to iDR3, the homogenization was carried out in a limited, exploratory way, based mostly on benchmark stars. During iDR4, the first full homogenization took place at all levels, making use of all the observed calibrators and of new homogenization algorithms. This effort provided important feedback on the calibration strategy, finalizing the calibrator selection strategy and the planning of the remaining calibration observations. The detailed homogenization procedure and algorithms are described in a companion paper (Hourihane et al., in prep., hereafter H17).

### 2.2. GES calibrator types and observing strategy

The GES calibrators fall into a few main groups that are described in more detail in the dedicated sections and are briefly

<sup>3</sup> This was not possible in all cases; for example, the hot star abundance nodes obviously relied on a different set of atmospheric models.

**Table 2.** List of GES iDR4 calibrators.

| CNAME            | Type | Field      | $J$<br>(mag) | $K$<br>(mag) |
|------------------|------|------------|--------------|--------------|
| 19250371+0049014 | CR   | Corot      | 11.27        | 10.47        |
| 21295872+1208321 | GC   | M15        | 11.78        | 11.39        |
| 11091266-5837236 | OC   | NGC 3532   | 11.63        | 11.32        |
| 07391749+0513163 | BM   | Procyon    | -9.99        | -9.99        |
| ssssssss-ssssss  | BM   | Sun        | -9.99        | -9.99        |
| 21534196-2840169 | RV   | HIP 108065 | -9.99        | -9.99        |

**Notes.** The full list is available at CDS. It can be used to select the iDR4 calibrators from the upcoming ESO Phase 3 public release. Here we show a portion to illustrate its contents. The columns contain (1) the GES unique identifier of each star (the CNAME), based on the object sexagesimal coordinates; (2) the calibration type, which can be GC or OC for clusters, RV for radial velocity standards, BM for benchmark stars, or CR for CoRoT targets; (3) the field name; (4) and (5) the 2MASS  $J$  and  $K$  magnitudes, when available.

summarized here. The iDR4 calibrators used here are listed in Table 2.

- Basic calibrations in GES are mostly related to RV standard star observations, as described in Sect. 3.
- In GES, we extend the set of calibrating objects by also including benchmark stars, in particular the *Gaia* FGK benchmark stars (Heiter et al. 2015b). They are carefully selected well-studied stars for which  $T_{\text{eff}}$  and  $\log g$  were derived as independently of spectroscopy as possible (i.e., based on interferometric diameters, parallaxes, etc., see Sect. 4 for more details). They are therefore good absolute calibrators of the parameters (i.e., for the accuracy) and useful references for the abundances.
- Like many other spectroscopic surveys, GES observes many stars belonging to OCs and GCs, as described in more detail in Sect. 5. These calibrators are quite powerful for checking the internal consistency of the abundance analysis (i.e., for the precision) and also provide a relatively reliable external reference for the abundance scale and AP determination.
- Collaborations are also ongoing with the CoRoT and *Kepler* teams to obtain accurate  $\log g$  reference values for large samples of giant stars, as described in Sect. 6.

The general idea behind the observing strategy is the following. For internal calibrations, each object should be observed with all the setups used by the different groups that will attempt a meaningful analysis of that object. For example, calibrators that can in principle be analyzed by OBA and FGK star experts should be observed with the setups adopted in GES for OBA stars (HR3, HR4<sup>4</sup>, HR5, HR6, and HR14) and FGK stars (HR9B, HR10, HR15N, and HR21). In another example, OCs contain stars with properties overlapping those of the MW field part of the survey. To ensure that OCs and field stars are analyzed consistently, a set of calibrating OCs should be observed with the cluster (HR9B and HR15N) and the field (HR10 and HR21) GIRAFFE setups. More details on the typically adopted setups for each calibration type can be found in the following sections and in Table 1.

To minimize the impact on the total observing time assigned by ESO, calibration observations are carried out as much as possible in twilight. This is generally appropriate for the brightest objects. Wavelength calibration lamps are switched on during

<sup>4</sup> This setup was introduced later to improve the  $\log g$  determination for hot stars, meaning that it was not employed for iDR4.

GIRAFFE observations for RV standards, while the usual GES procedure of inserting short exposures with the lamps on is employed for benchmarks and cluster observations, to avoid spoiling scientific exposures with scattered light from lamps.

All calibration data are reduced in the same way as any other GES observation to extract the final science-ready spectra. The ESO processing pipelines (Ballester et al. 2000) are employed to produce extracted and wavelength-calibrated UVES spectra, while a dedicated pipeline for the GIRAFFE processing was developed at the Cambridge Astronomy Survey Unit<sup>5</sup> (CASU). Both pipelines are complemented with GES-specific software to perform additional operations such as sky subtraction or continuum normalization, and radial velocity determination (for more details, see Jeffries et al. 2014; Sacco et al. 2014, for GIRAFFE and UVES, respectively).

### 3. Basic calibrators

In addition to the acquisition of an adequate set of calibration frames such as bias, flat fields, wavelength calibration lamps, and sky fibers placement<sup>6</sup>, basic spectroscopic calibrations generally include the observation of flux standard stars, RV standard stars, and hot, fast-rotating stars for telluric absorption band removal, also referred to as telluric standard stars.

For a large spectroscopic survey like GES, where the main deliverables are chemical abundances, RVs, and APs, the flux calibration of spectra is not a crucial requirement and is therefore not performed. The correction for telluric absorption features is likewise not crucial, especially because it only affects the very last portion of HR21 GIRAFFE spectra and short-wavelength intervals in the UVES spectra<sup>7</sup>. If it will become necessary for specific scientific applications, telluric absorption bands can be efficiently removed in future GES releases with the use of Earth atmospheric models (for example, from the TAPAS collaboration, Bertaux et al. 2014). Therefore, no observations of telluric standards were carried out over the current survey, and none are planned overall.

Accurate and precise RV measurements are one of the main tools to fulfill the scientific goals of GES, and to this end, a specific calibration strategy was implemented.

#### 3.1. Radial velocity standard stars

GES requires radial velocities with a precision in the range 0.3–1.0 km s<sup>-1</sup> to fulfill its various scientific goals (Gilmore et al. 2012), and both UVES and GIRAFFE have the potential of delivering RVs with a precision well below 500 m s<sup>-1</sup> (see also Sacco et al. 2014; Jackson et al. 2015). To reach an accuracy comparable to the quoted precision, it is necessary to keep the systematics under control, especially those related to the wavelength calibration scale, the non-uniform fiber or slit illumination, and the template mismatch in the cross-correlation procedure.

To greatly reduce the systematics associated with the wavelength calibration, it was sufficient for GIRAFFE to associate

<sup>5</sup> <http://www.ast.cam.ac.uk/~mike/casu/>

<sup>6</sup> For young clusters or objects where the sky is expected to vary significantly across the FLAMES field of view, the sky fibers positioning and sky subtraction method are crucial.

<sup>7</sup> Some key diagnostics such as the forbidden oxygen line at 6300 Å are indeed affected by telluric absorption, and therefore we anticipate that a correction for telluric bands will be necessary for a detailed study of these diagnostics.

**Table 3.** Radial velocity standards for zero-point calibration of GES, with their reference RV measurements, taken from [Soubiran et al. \(2013\)](#) except for GJ 388 ([Chubak et al. 2012](#)).

| ID         | Type       | V<br>(mag) | RV<br>(km s <sup>-1</sup> ) | $\delta$ RV<br>(km s <sup>-1</sup> ) |
|------------|------------|------------|-----------------------------|--------------------------------------|
| GJ 388     | M4.5       | 9.43       | 12.453                      | 0.066                                |
| HIP 616    | K0V        | 8.70       | -42.994                     | 0.009                                |
| HIP 5176   | G0         | 8.15       | 10.366                      | 0.006                                |
| HIP 85295  | K7V        | 7.54       | -23.422                     | 0.016                                |
| HIP 17147  | F9V        | 6.68       | 120.400                     | 0.007                                |
| HIP 20616  | G0         | 8.41       | 38.588                      | 0.009                                |
| HIP 26335  | K7         | 8.78       | 21.772                      | 0.006                                |
| HIP 26973  | K0V        | 8.52       | 26.600                      | 0.006                                |
| HIP 29295  | M1/M2V     | 8.15       | 4.892                       | 0.009                                |
| HIP 31415  | F6V        | 7.70       | -7.479                      | 0.012                                |
| HIP 32045  | K5         | 8.49       | 40.722                      | 0.007                                |
| HIP 32103  | G5/G6IV/V  | 8.53       | 27.167                      | 0.006                                |
| HIP 33582  | G0         | 9.02       | -94.239                     | 0.006                                |
| HIP 38747  | G5         | 8.37       | -8.002                      | 0.007                                |
| HIP 45283  | G2V        | 8.01       | 39.451                      | 0.005                                |
| HIP 47513  | M2         | 10.38      | 11.626                      | 0.007                                |
| HIP 47681  | G5V        | 8.41       | 11.289                      | 0.007                                |
| HIP 50139  | G1V        | 7.75       | -21.976                     | 0.005                                |
| HIP 51007  | M0         | 10.15      | 21.758                      | 0.006                                |
| HIP 58345  | K4V        | 6.99       | 48.605                      | 0.009                                |
| HIP 65859  | M1V        | 9.05       | 14.386                      | 0.009                                |
| HIP 66032  | K2IV/Vp... | 9.17       | 4.126                       | 0.009                                |
| HIP 77348  | G5         | 8.05       | 1.907                       | 0.011                                |
| HIP 80423  | G3/G5Vw... | 9.32       | -42.148                     | 0.006                                |
| HIP 85295  | K7V        | 7.54       | -23.422                     | 0.016                                |
| HIP 93373  | G8V        | 8.60       | -91.911                     | 0.006                                |
| HIP 104318 | G5         | 8.01       | 4.910                       | 0.006                                |
| HIP 105439 | K0 III+... | 6.75       | 17.322                      | 0.006                                |
| HIP 106147 | K4/K5V     | 9.11       | -84.533                     | 0.009                                |
| HIP 108065 | K0/K1III+. | 7.82       | -41.660                     | 0.010                                |
| HIP 113576 | K5/M0V     | 7.88       | 16.138                      | 0.010                                |

with the scientific exposures short adjacent exposures with the the simultaneous wavelength calibration lamp (SIMCAL) switched on. The use of sky lines can also improve the RV accuracy, as shown by [Jeffries et al. \(2006\)](#) and [Koposov et al. \(2011\)](#). To reach an even better accuracy (better than  $\approx 300$  m s<sup>-1</sup>) the repeated observation of RV standards of different spectral types with the specific purpose of calibrating the RV zero point is necessary. For UVES, the use of sky lines has proved to reach a sufficient zero-point accuracy, therefore no more UVES observations of RV standards were required starting from 2015, while they are continuing for GIRAFFE. More details on the wavelength and RV calibration strategy for GIRAFFE and UVES spectra can be found in [Jeffries et al. \(2014\)](#) and [Sacco et al. \(2014\)](#), respectively, and in the GES description papers (Gilmore et al.; Randich et al., in prep.).

GES was conceived to achieve its maximum impact once combined with *Gaia* data (Sect. 1), therefore the main source of RV standards for GES was the *Gaia* standard star catalog ([Soubiran et al. 2013](#)), complemented by [Chubak et al. \(2012\)](#). We relied on the best RV calibrators found in the *Gaia* catalog that appeared to be stable in RV within a few m s<sup>-1</sup> over the explored time baseline (see Table 3 for a list of targets). Later, after the processing of the first internal data release (iDR1), the need for more RV stars cooler than  $\approx 4000$  K emerged, and four M stars were included into the list. No hot standards are included

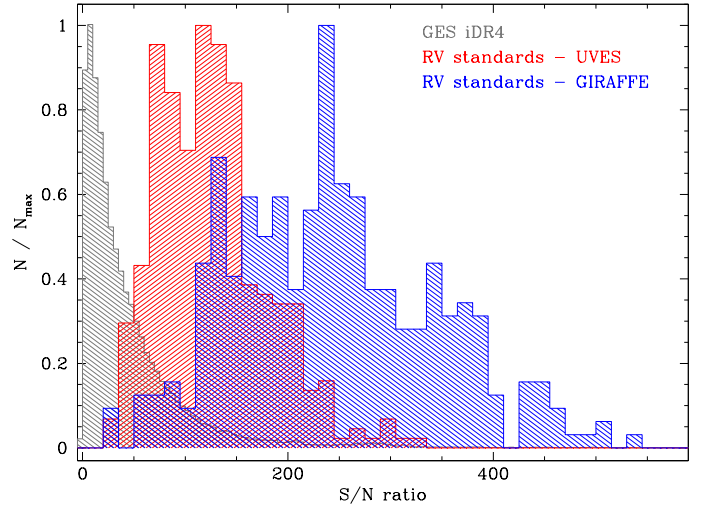


**Fig. 5.** S/N of individual spectra of RV standards for the RV zero point calibration. There are between 2 and 20 spectra per star, typically 10. The UVES setup used is 580 (see Table 1) and the GIRAFFE setups are HR9B, HR10, 15N, and 21. The very high S/N are due to the RV standard brightness (see Table 3) and to the need of integrating for relatively long exposure times to average out illumination non-homogeneities within the fibers.

in the calibration set. We are observing one or two RV standards in every observing run (approximately once per month). We used relatively long exposure times (about 100 s) compared to other bright calibrators such as benchmark stars, and avoided saturation not only to increase the S/N (see Fig. 5), but also to ensure uniform slit illumination, and with the SIMCAL on when observing with GIRAFFE.

In addition to being used to set the zero-point of GIRAFFE RV measurements, the RV standards are also used in the WG15 homogenization procedure, which is described in detail by H17. Briefly, the performance of each of the observed setups was tested with RV standards (see Fig. 6) to identify the setups that show the smallest offset with respect to the reference values of Table 3. All other setups were corrected to the scale of the best setup (generally HR10, followed by HR15N) using the stars in common with the best available setup to compute an offset. In previous GES releases, offsets of  $\approx 0.5$  km s<sup>-1</sup> were reported between UVES and GIRAFFE (see [Sacco et al. 2014](#); [Donati et al. 2014](#); [Lardo et al. 2015](#), among others). In iDR4, the two instruments showed much smaller differences, of a few meters per second, thanks to the use of sky lines to correct for UVES wavelength calibration uncertainties. The setup that shows the largest offset is HR21 ( $\approx 0.5$  km s<sup>-1</sup>), for which the SIMCAL lamps are switched off to avoid contaminating the scientific exposure given the high efficiency of this particular setup.

#### 4. Benchmark stars

In traditional works of stellar abundance analysis, the Sun is used as a reference, either to verify a posteriori the validity of the presented results by performing an analysis of a solar spectrum with the same technique employed on the program stars, or to perform a differential analysis of the program stars with respect to the Sun (see [Sousa et al. 2014](#), for a GES-related example of this type of analysis). A second example of a reference star widely used for testing abundance analysis of cooler, more metal-poor stars is Arcturus (see, e.g., [Ramírez & Allende Prieto 2011](#); [Mészáros et al. 2013](#); [Morel et al. 2014](#), and included

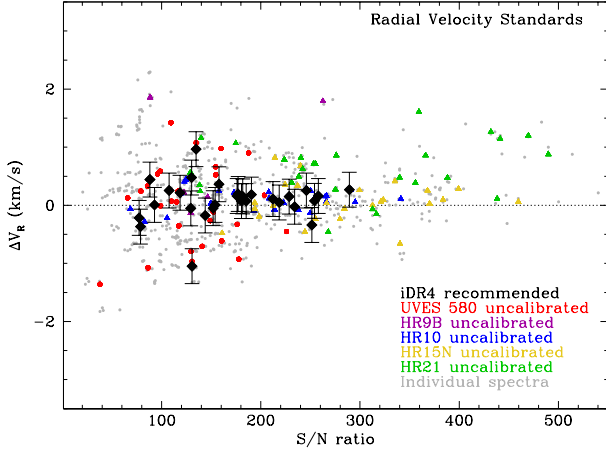


**Fig. 6.** Example of the result of RV homogenization on RV standards. Gray dots show the difference between individual spectrum measurements and the reference values of Table 3. The colored symbols are the same RV differences, but aggregated for each RV standard star in the various setups, and are still uncalibrated. The final iDR4 recommended values, obtained from the internal homogenization process, are shown by large black diamonds, which are placed at the average S/N of the spectra obtained for each RV standard star.

references). Moreover, when large samples are analyzed, the stars in common of different literature studies are used as a comparison to put all data on the same system, as much as possible (see, e.g., [Worley et al. 2012](#); [De Pascale et al. 2014](#); [Bensby et al. 2014](#)). Within the *Gaia* mission preparatory effort, the concept of one reference star for APs determination and abundance analysis verification has been extended to define the so-called *Gaia* benchmark star set ([Heiter et al. 2015b](#)). Benchmark stars ideally have known HIPPARCOS parallaxes, angular diameters, and bolometric fluxes, and their masses have been determined in a homogeneous way, so that their effective temperatures and surface gravities can be derived as independently of spectroscopy as possible.

Even though FLAMES is not the ideal instrument to observe individual stars, it was deemed extremely important to observe these fundamental reference objects within GES. Because they are bright stars, they were observed mainly during twilight, with the three GES UVES setups and with the GIRAFFE HR9B, 10, 15N, and 21 setups (see Table 1), that is to say, the four GES setups used for FGK stars in the MW field and in OCs. GES furthermore extended the list to also include a few cooler K and M benchmarks and a few hotter O, B, and A benchmarks, as detailed in the next sections. The hot benchmark stars were also observed with the GES hot stars GIRAFFE setups: HR3, 5A, 6, and 14A (see Table 1). The S/N of the observed spectra is reported in Fig. 7.

Benchmark stars and candidate benchmarks are used both in the WG-level and survey-level homogenization processes to assess which abundance analysis nodes and WGs, respectively, perform better in different regions of the parameters space, as expanded in Sect. 4.4. More details on the use of benchmark stars can be found in [Smiljanic et al. \(2014\)](#), [Lanzafame et al. \(2015\)](#), and H17.

#### 4.1. *Gaia* FGK benchmarks

The FGK benchmark stars that were selected as GES astrophysical calibrators are listed in Table 4. They are extracted from the original set of *Gaia* FGK benchmark stars ([Heiter et al. 2015b](#)),

**Table 4.** *Gaia* FGK benchmark stars observed in GES.

| ID                     | Type     | <i>V</i><br>(mag) | [Fe/H] <sub>NLTE</sub><br>(dex) | <i>T</i> <sub>eff</sub><br>(K) | log <i>g</i><br>(dex) |
|------------------------|----------|-------------------|---------------------------------|--------------------------------|-----------------------|
| Procyon                | F5IV-V   | 0.366             | +0.01                           | 6545                           | 4.00                  |
| HD 84937               | sdF5     | 8.324             | -2.03                           | 6275                           | 4.06                  |
| HD 49933               | F2V      | 5.762             | -0.41                           | 6635                           | 4.21                  |
| δ Eri                  | K1III-IV | 3.527             | +0.06                           | 5045                           | 3.76                  |
| HD 140283              | sdF3     | 7.210             | -2.36                           | 5720                           | 3.67                  |
| ε For                  | K2V      | 5.883             | -0.60                           | 5069                           | 3.45                  |
| η Boo                  | G0IV     | 2.681             | +0.32                           | 6105                           | 3.79                  |
| β Hyi                  | G0V      | 2.797             | -0.04                           | 5873                           | 3.98                  |
| α Cen A                | G2V      | 0.002             | +0.26                           | 5847                           | 4.31                  |
| HD 22879               | F9V      | 6.689             | -0.86                           | 5786                           | 4.23                  |
| Sun                    | G2V      | -26.74            | 0.00                            | 5771                           | 4.44                  |
| τ Cet                  | G8.5V    | 3.495             | -0.49                           | 5331                           | 4.44                  |
| α Cen B                | K1V      | 1.357             | +0.22                           | 5260                           | 4.54                  |
| 18 Sco                 | G2Va     | 5.505             | +0.03                           | 5747                           | 4.43                  |
| μ Ara                  | G3IV-V   | 5.131             | +0.35                           | 5845                           | 4.27                  |
| β Vir                  | F9V      | 3.608             | +0.24                           | 6083                           | 4.08                  |
| Arcturus               | K1.5III  | -0.051            | -0.52                           | 4247                           | 1.60                  |
| HD 122563              | F8IV     | 6.200             | -2.64                           | 4587                           | 1.61                  |
| ε Vir                  | G8III    | 2.828             | +0.15                           | 4983                           | 2.77                  |
| ξ Hya                  | G7III    | 3.541             | +0.16                           | 5044                           | 2.87                  |
| α Tau                  | K5III    | 0.867             | -0.37                           | 3927                           | 1.22                  |
| ψ Phe                  | M4III    | 4.404             | -1.24                           | 3472                           | 0.62                  |
| γ Sge                  | M0III    | 3.476             | -0.17                           | 3807                           | 1.05                  |
| α Cet                  | M1.5IIIa | 2.526             | -0.45                           | 3796                           | 0.91                  |
| β Ara <sup>a</sup>     | K3Ib-II  | 2.842             | -0.05                           | 4197                           | 1.05                  |
| HD 220009 <sup>a</sup> | K2III    | 5.047             | -0.74                           | 4217                           | 1.43                  |
| HD 107328              | K0IIIb   | 4.970             | -0.33                           | 4496                           | 2.09                  |
| ε Eri                  | K2Vk:    | 3.726             | -0.09                           | 5050                           | 4.60                  |

**Notes.** Magnitudes and APs are from [Heiter et al. \(2015b\)](#), NLTE-corrected metallicities from [Jofré et al. \(2014\)](#). <sup>(a)</sup> Not recommended as benchmarks from iDR5 on.

which contains 34 stars with *T*<sub>eff</sub> in the range ≈3500–6500 K, log *g* in ≈0.5–4.5 dex, and with a metallicity ranging from super-solar to -2.5 dex. Additional spectra of these stars were gathered from the ESO archive (UVES and HARPS) and from the NARVAL archival observations at the Pic du Midi, and homogenized into a comprehensive library of high-resolution spectra ([Blanco-Cuaresma et al. 2014](#)). The only fundamental parameter that was not well constrained for these stars in the literature was [Fe/H], therefore an effort from the GES abundance analysis nodes was made to independently derive a set of reference [Fe/H] values for each of them ([Jofré et al. 2014, 2015](#)), along with abundances for ten elements, as a first step. Figure 8 gives an idea of the parameter space covered by the *Gaia* benchmark stars. The set only contains a few metal-poor stars, a regime that is not much sampled in GES (see Fig. 2), but we recently identified a few more candidates with [Fe/H] < -1.2 dex ([Hawkins et al. 2016](#)).

#### 4.2. Additional M benchmarks

The collection of *Gaia* benchmark stars from which we selected the sample described in the previous section does not include a sufficient number of stars cooler than ≈3500 K. Benchmark stars in the M-dwarf region are needed both for *Gaia* (expected to observe more than one million M dwarfs) and GES, where M dwarfs are included in OC target stars. Angular diameter

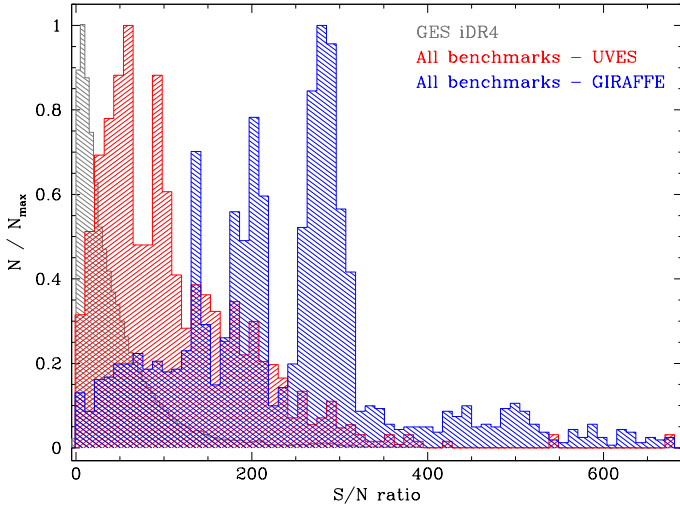


**Fig. 7.** S/N of individual spectra of benchmark stars. In an initial phase, spectra were obtained in a range of S/N values. Later, we aimed at obtaining at least three exposures per benchmarks star per setup, with a combined  $S/N > 100$  per pixel (without saturating).

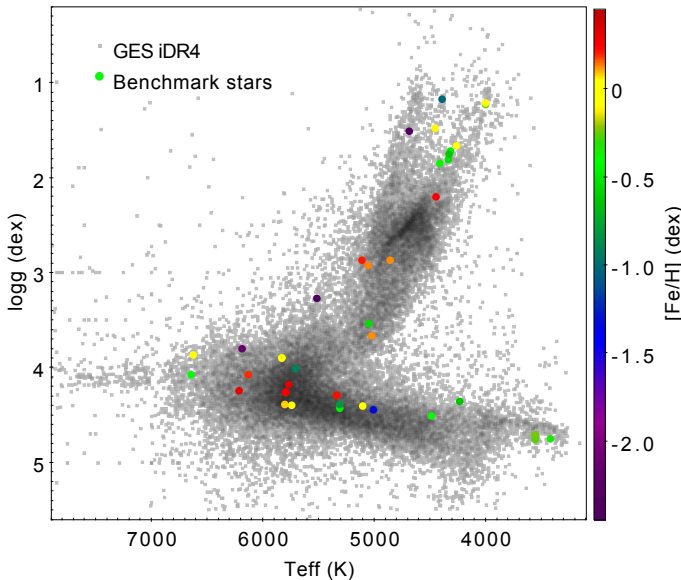


**Fig. 8.** Position on the  $T_{\text{eff}} - \log g$  plane of the *Gaia* FGK benchmark stars (Heiter et al. 2015b, see also Sect. 4.1) analyzed in iDR4, colored according to their [Fe/H]. A few of the cooler benchmarks ( $T_{\text{eff}} < 4000$  K) described in Sect. 4.2 were also analyzed in iDR4. The whole GES iDR4 sample is reported in the background as smaller grey squares.

measurements for potential cool benchmark stars have only recently started to become available, and homogeneous metallicity determinations for the most promising ones are not available yet.

Nevertheless, we selected a number of candidate benchmarks among the best studied M-dwarf stars, listed in Table 5. For four of these stars, angular diameters were published by Boyajian et al. (2012) with a precision of 1–2%, while the angular diameters of GJ 436 and GJ 581 were determined by von Braun et al. (2011, 2012) to 3%, and that of GJ 551 by Demory et al. (2009) to 5%. Bolometric fluxes were measured for all stars by Boyajian et al. (2012) with a precision of 1%. These data give  $T_{\text{eff}}$  independent of photometry or spectroscopy for all stars, as listed in Table 5. Spectroscopic metallicity determination is more difficult for M dwarfs than for FGK dwarfs because of the more

**Table 5.** Additional M-dwarf benchmark stars, with their magnitudes and spectral type from SIMBAD, metallicities as noted, and  $T_{\text{eff}}$  from Boyajian et al. (2012).

| ID                  | Type  | $V$<br>(mag) | [Fe/H]<br>(dex)    | $T_{\text{eff}}$<br>(K) | Status |
|---------------------|-------|--------------|--------------------|-------------------------|--------|
| GJ 205              | M1.5V | 7.97         | +0.35 <sup>a</sup> | 3801                    | iDR3   |
| GJ 436              | M3V   | 10.59        | +0.03 <sup>b</sup> | 3416                    | iDR4   |
| GJ 526              | M1.5V | 8.50         | −0.30 <sup>a</sup> | 3618                    | iDR4   |
| GJ 551 <sup>c</sup> | M5.5V | 11.05        | +0.24 <sup>d</sup> | 3054                    | –      |
| GJ 581              | M2.5V | 10.61        | −0.02 <sup>b</sup> | 3442                    | iDR4   |
| GJ 699              | M4V   | 9.51         | −0.39 <sup>a</sup> | 3224                    | iDR3   |
| GJ 880              | M1.5V | 8.64         | +0.03 <sup>e</sup> | 3713                    | iDR2   |

**Notes.** <sup>(a)</sup> Metallicity from Rojas-Ayala et al. (2012). <sup>(b)</sup> Metallicity from Lindgren et al. (2016). <sup>(c)</sup> Not observed yet, we rely on UVES archival data. <sup>(d)</sup> Metallicity from Jofré et al. (2014), considering  $\alpha$  Cen A and B. <sup>(e)</sup> Metallicity from Neves et al. (2014).

complex optical spectra. Several approaches have been pursued in the literature. These include calibrations of photometric data or low-resolution infrared spectroscopic features (e.g., Rojas-Ayala et al. 2012), or analysis of high-resolution spectra in optical or infrared regions (e.g., Önehag et al. 2012; Neves et al. 2014; Lindgren et al. 2016). Usually, samples of binaries with M and FGK components are used for calibration or validation of the methods. Selected metallicities from various sources are listed in Table 5.

For most of these stars, additional high-resolution spectra are available together with those obtained with the GES setups. GJ 436, GJ 526, and GJ 880 were observed at optical and near-IR wavelengths with the NARVAL spectrograph. For GJ 436, GJ 551, GJ 581, and GJ 880,  $J$ -band spectra with  $R = 50\,000$  were obtained with the CRIRES spectrograph at the VLT. GJ 699 is included in the CRIRES-POP library (wavelength range from 1 to 5  $\mu\text{m}$ , Lebzelter et al. 2012). These high-quality archival data constitute a legacy sample that will allow us to compare results obtained in the optical and infrared wavelength regions. In GES iDR4 all observations for the listed cool benchmarks were completed, except for GJ 551 (Proxima Centauri), for which we will most probably have to rely on UVES archival data in future data releases.

### 4.3. Additional OBA benchmarks

While benchmarks stars with APs as independent as possible from spectroscopy are becoming available for FGK and M types, as we discussed above, the situation is not as favorable in the case of hotter stars. This is due to the lack of interferometric data and the lack of spectrophotometry in the ultraviolet where the flux of these stars dominates. With this limitation in mind, we can, however, define a sample of well-studied A, B, and O-type stars with relatively well-established parameters in the refereed literature, even if not independent of spectroscopy.

For the calibration of APs of A-type stars, we selected five benchmark stars previously observed for the AP calibration of hot stars for *Gaia* (Bailer-Jones et al. 2013). These *Gaia* benchmark stars were observed with  $S/N \approx 1000$ , using the Hermes spectrograph at the Mercator telescope ( $R = 85\,000$ ) in La Palma, Spain. Additional *Gaia* OBA benchmark spectra are being observed in ongoing dedicated observing programs. We complemented the set with one late B-type star with

$T_{\text{eff}} \approx 11\,000\text{ K}$  (134 Tau). These stars were carefully selected to cover different spectral subtypes, to have low  $v \sin i$  values, and to be bright and visible from Paranal. Their optical spectra show sufficiently deep and narrow absorption lines in the wavelength regions that are also observed by GES. They are currently being observed by GES and will be used not only for survey-level homogenization, but also to test the quality of APs and elemental abundance computed by the WG13 nodes for all GES A- and late B-type stars in various Galactic young OCs.

For the early B-type stars, the selected pool of candidate benchmarks had their parameters ( $T_{\text{eff}}$  and  $\log g$ ) estimated solely from high-resolution spectroscopic data (e.g., this excludes  $T_{\text{eff}}$  measurements based on photometric indices). In addition, only studies treating the line formation in non-local thermal equilibrium (non-LTE) were considered. The model atmospheres used may be either LTE or non-LTE (LTE being a reasonable assumption for B-type dwarfs; Przybilla et al. 2011), but a full line blanketing was considered a requirement. We performed a comparison of the available studies for each candidate B-type benchmark for GES and rejected discrepant measurements (e.g., a few of the very high gravities from Daflon & Cunha 2004, and references therein). In some cases, stars were studied by various authors with similar data and methods, but we preferred one set over another to avoid redundancies. For example, we used the results of Nieva & Przybilla (2012) for the four stars in common with Nieva & Simón-Díaz (2011), or for the three stars in common with Irrgang et al. (2014). The stars eventually selected have consistent APs from at least two high-quality and independent studies. It is important to note that most B stars analyzed by GES that also generally belong to young OCs are fast rotators (e.g.,  $\langle v \sin i \rangle \sim 160\text{ km s}^{-1}$  in NGC 3293). In contrast, the abundance studies in the literature are heavily biased against such objects. As a consequence, the vast majority of the selected B benchmark stars are slow rotators (by far the fastest rotator is  $\theta$  Car with  $v \sin i \sim 110\text{ km s}^{-1}$ ; Hubrig et al. 2008). This caveat should be kept in mind.

The O-type candidate benchmarks were selected from the new Galactic O-star spectroscopic survey spectral classification standard grid (Maíz Apellániz et al. 2015), which is a recent revision of the atlas for spectral classification, first established by Walborn & Fitzpatrick (1990). The full grid comprises more than 100 stars with spectral subtypes from O2 to O9.7 and luminosity classes from V to Ia in both hemispheres, and it has been observed at high resolution ( $R \approx 50\,000$ ) in two dedicated surveys (OWN and IACOB, see Barbá et al. 2010, 2014; Simón-Díaz et al. 2011a,b, 2015). A quantitative and homogeneous spectroscopic analysis of the OWN and IACOB samples is being performed within the framework of the IACOB project, and the results will soon be published (Holgado et al., in prep.), along with the full spectrum library. The multi-epoch spectra of the OWN and IACOB projects also allow for variability searches, and a literature comparison with recent hot star surveys results for  $v \sin i$ ,  $T_{\text{eff}}$ ,  $\log g$ , and helium abundance (Repolust et al. 2004; Markova et al. 2014; Martins et al. 2015) is also being carried out.

Table 6 lists the OBA candidate benchmarks observed by GES up to now, while Fig. 9 shows the parameter coverage of the observed and candidate OBA benchmarks in the  $T_{\text{eff}} - \log g$  plane. We expect to observe a few more OBA benchmarks before the end of the survey.

#### 4.4. GES benchmarks results

Benchmark stars were used in GES iDR4 within each WG to homogenize the results of different abundance analysis nodes

**Table 6.** List of OBA benchmark candidates observed by GES. None were analyzed in any internal release so far.

| Star                              | V (mag) | Type     | $T_{\text{eff}}$ (K) | $\log g$ (dex) | Status   |
|-----------------------------------|---------|----------|----------------------|----------------|----------|
| HD 93128 <sup>a</sup>             | 6.90    | O3.5V    | 49 300               | 4.10           | started  |
| HD 319699 <sup>a</sup>            | 9.63    | O5V      | 41 200               | 3.91           | started  |
| HD 163758 <sup>a</sup>            | 7.32    | O6.5Iafp | 34 600               | 3.28           | observed |
| HD 68450 <sup>a</sup>             | 6.44    | O9.7II   | 30 600               | 3.30           | observed |
| $\tau$ Sco <sup>b,c,d,e,f,g</sup> | 2.81    | B0.2V    | 31 750               | 4.13           | observed |
| $\theta$ Car <sup>c,d</sup>       | 2.76    | B0Vp     | 31 000               | 4.20           | observed |
| $\gamma$ Peg <sup>b,c,h</sup>     | 2.84    | B2IV     | 22 350               | 3.82           | observed |
| HD 56613 <sup>c</sup>             | 7.21    | B8V      | 13 000               | 3.92           | observed |
| 134 Tau <sup>i</sup>              | 4.87    | B9IV     | 10 850               | 4.10           | observed |
| 68 Tau <sup>j</sup>               | 4.31    | A2IV     | 9 000                | 4.00           | observed |

**Notes.** A few more OBA stars will be observed before the end of the survey. Magnitudes and spectral types are from SIMBAD.

**References.** References for APs: <sup>(a)</sup> Holgado et al., in prep. (see text); <sup>(b)</sup> Nieva & Przybilla (2012); <sup>(c)</sup> Lefever et al. (2010); <sup>(d)</sup> Hubrig et al. (2008); <sup>(e)</sup> Simón-Díaz et al. (2006); <sup>(f)</sup> Mokiem et al. (2005); <sup>(g)</sup> Martins et al. (2012); <sup>(h)</sup> Morel & Butler (2008); <sup>(i)</sup> Smith & Dworetzky (1993); <sup>(j)</sup> Burkhardt & Coupry (1989).

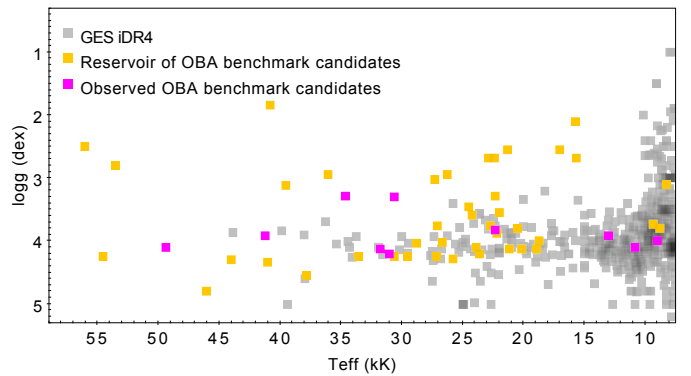


**Fig. 9.** Position of OBA benchmark candidates on the  $T_{\text{eff}} - \log g$  plane. The OBA benchmarks are plotted as magenta squares; the pool of OBA benchmarks from which a few more will be selected for observations is represented by yellow squares; the GES iDR4 sample is reported in the background as gray squares.

(see, e.g. Smiljanic et al. 2014) and at the survey level to homogenize the results of different WGs (see H17). Additionally, in iDR4, the FGK benchmark stars are among the few calibrators that are also used to provide an external reference for APs, that is, they are used as it absolute calibrators. For example, WG11 defines weights for each of the abundance analysis node results, which vary for different regions of the AP space based on that node's results on benchmark stars. The calibration procedures derived using benchmarks, among other calibrators, are applied to all survey data, and therefore it is useful to examine the effects of the whole process on the benchmark stars themselves. Figure 10 shows differences of the iDR4 recommended GES APs and  $[\text{Fe}/\text{H}]$  values with the reference AP values (Heiter et al. 2015b) and NLTE metallicities (Jofré et al. 2014). The average differences are  $T_{\text{eff}} = 14 \pm 113\text{ K}$ ,  $\log g = -0.07 \pm 0.19\text{ dex}$ , and  $[\text{Fe}/\text{H}] = -0.02 \pm 0.13\text{ dex}$ . In all cases, the average offsets are negligible, and the dispersions give an idea of the typical GES performances on these high S/N spectra.

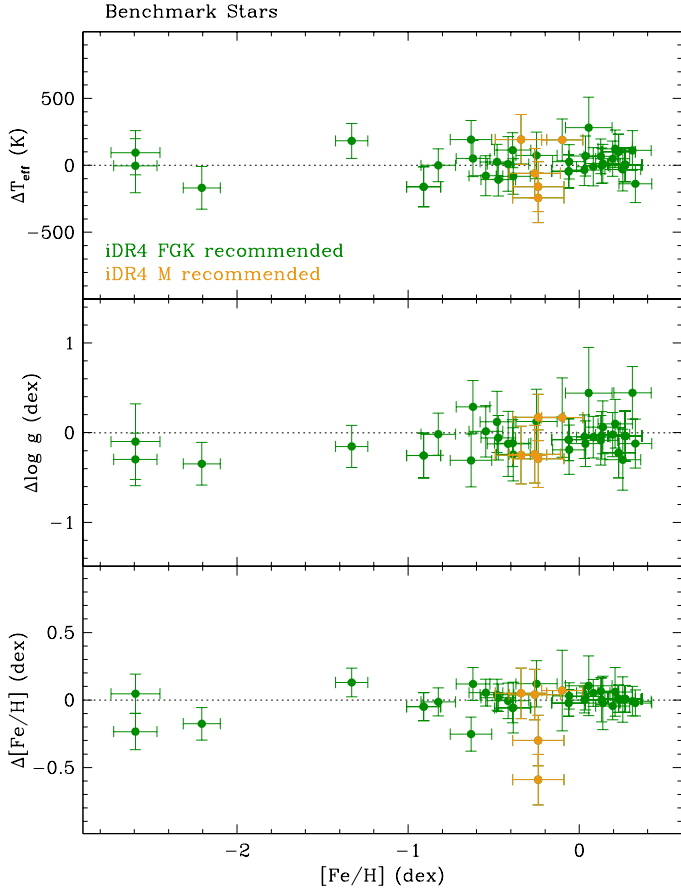


**Fig. 10.** Comparison of GES iDR4 recommended values with the reference APs (Heiter et al. 2015b) and  $[\text{Fe}/\text{H}]$  (Jofré et al. 2014) values. In all panels, FGK benchmark stars are plotted in green and M benchmarks in orange. All differences are in the sense GES minus reference.

## 5. Star clusters

Often, the goal of providing astrophysical calibrations for a spectroscopic survey is achieved by observing clusters in the MW. Both relatively old OCs (Sect. 5.1), and GCs (Sect. 5.3) are used in various surveys (RAVE, GALAH, and APOGEE, for example). They are extremely powerful calibrators of APs and abundance ratios for a number of reasons:

- although their APs are not as accurate as those of benchmark stars (Sect. 4), clusters contain many stars with similar (to first order) distances, ages, and chemical compositions<sup>8</sup>; thus, clusters provide extremely robust calibrators because they also provide a way to statistically estimate the uncertainty on determined metallicities and abundance ratios;
- both OCs and GCs can globally rely upon a vast literature of photometric, astrometric, and spectroscopic measurements, and on very advanced models of stellar structure and evolution, which are invaluable tools, making clusters ideal reference objects for external calibration and literature cross-checks;
- having stars with virtually the same distance, it is possible to precisely know the surface gravity, which is one of the most

<sup>8</sup> With caution on some light (C, N, O, Na, Mg) and s-process elements, which can vary significantly in GC stars (see, e.g., Gratton et al. 2012). Spreads in  $[\text{Fe}/\text{H}]$  are also observed or claimed in a few GCs. This needs to be duly taken into account when using these clusters as calibrators.

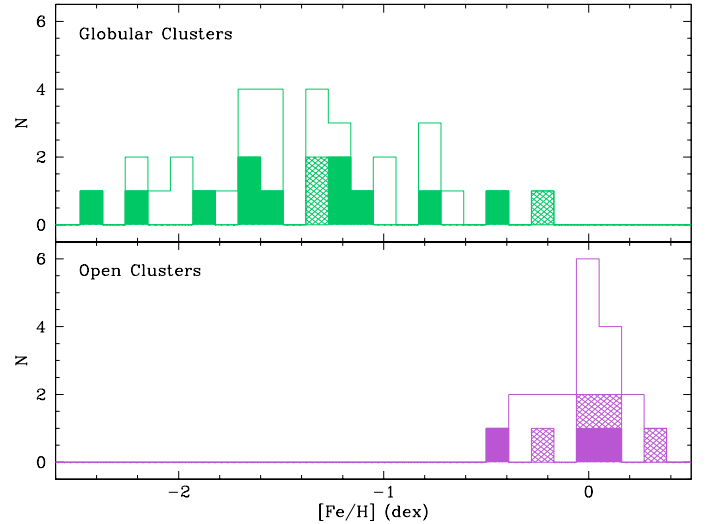


**Fig. 11.** Metallicity distribution of calibrating clusters: the top panel shows GCs and the bottom panel OCs. Heavily shaded histograms show clusters included in iDR4; lightly shaded histograms clusters that will be included in future releases (see also Tables 8 and 7); empty histograms represent a pool of viable candidates to complete the coverage. A few of them might be selected in the next observing runs, depending on observations scheduling and data homogenization needs.

difficult quantities to derive for field stars without an absolute distance determination (see also Sect. 6); in general, it is possible to derive precise APs from the many high-quality photometric catalogs available, therefore clusters also provide an invaluable testbench for the AP determination of a survey;

- cluster stars have different APs, which vary along the sequences of the color-magnitude diagram in a regular way, allowing for the investigation of chemical abundance trends with parameters: no other calibrator allows for this type of a check of the internal consistency of an abundance analysis, which is invaluable even for each individual method, even before comparing different methods;
- finally, the AP variations of cluster stars allows for a very efficient internal calibration of a complex survey like GES because they have the same metallicity; in particular, they allow the linking of various abundance analysis techniques employed by the many GES abundance analysis nodes for giants and dwarfs, cool and hot stars, and GIRAFFE and UVES spectra.

Star clusters in iDR4 were not used as absolute (external) calibrators like benchmark stars, but were rather used a posteriori to verify the quality of the whole homogenization procedure at the node, WG, and survey levels (see also Sect. 5.5). The metallicity range covered by GES calibrating clusters is presented in Fig. 11, while Fig. 12 shows the distribution of S/N for individual spectra, where typically each star was observed three times per setup.

### 5.1. OC selection criteria

Calibrating OCs<sup>9</sup> were selected to interface with other current spectroscopic surveys, including also well-known and often

<sup>9</sup> Calibrating OCs here means those OCs (or OC stars) that are observed specifically for the purpose of calibration, that is, with both the MW field and the OC setups. Many more OC stars and OCs are observed for GES scientific purposes, and these are called science OCs. Generally, the calibrating OC stars are a subset of the science OCs.

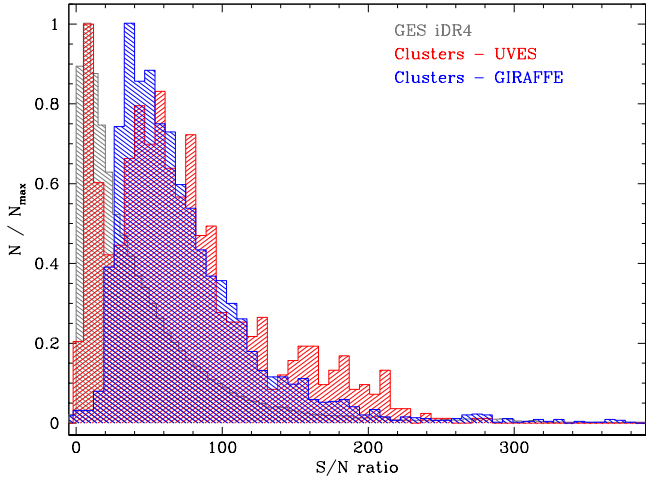


**Fig. 12.** S/N of individual spectra of calibrating cluster stars in open and globular clusters. There are typically  $>3$  exposures per star per setup. The required S/N per star after combining at least three spectra per star was  $>50$ , thus individual exposures peak roughly around 30–40 for GIRAFFE, who was driving the total exposure time. A tail of low S/N spectra for UVES contains mostly archival spectra of subgiants and MS stars.

studied clusters, to cover the metallicity range of interest. In the case of OCs, however, we tried to use as much as possible the targets selected by the GES OC group, because they have gathered the most recent literature data in terms of photometry, membership, binarity, and so on (see Bragaglia et al., in prep., for more details), and because we could profit from the GES analysis to further select more reliable members. This is also the reason why calibrating OC observations started later in the survey than calibrating GC observations.

We gave priority to relatively old OCs with a red clump<sup>10</sup>, so that in many calibrating OCs we have both red clump giants and main-sequence dwarfs. The GES science target OCs are generally observed with the UVES 580 setup and the GIRAFFE HR15N and HR9B setups (see Table 1). Additionally, the stars selected for calibrations were also observed with the HR10 and HR21 GIRAFFE setups, that is, with those used for MW field stars. This was intended to facilitate the internal calibration and to increase the wavelength coverage, thus making the abundance analysis of calibrating stars more reliable.

In iDR4, three OCs were observed, as indicated in Table 7, while four more were completed recently. Additional OCs may be added in the future, depending on scheduling and analysis requirements.

## 5.2. Selection criteria for individual OC stars

For OCs, the individual star selection criteria varied from case to case. The reliable members observed with the OC and field setups that are also included in iDR4 are displayed in Fig. 13. Our main guidelines were

- to profit from the target selection effort performed by the GES OC group (Bragaglia et al., in prep.) by selecting the candidates among stars that already had good membership information from the literature, or from previous GES internal releases; in other words, for most calibrating OCs, the

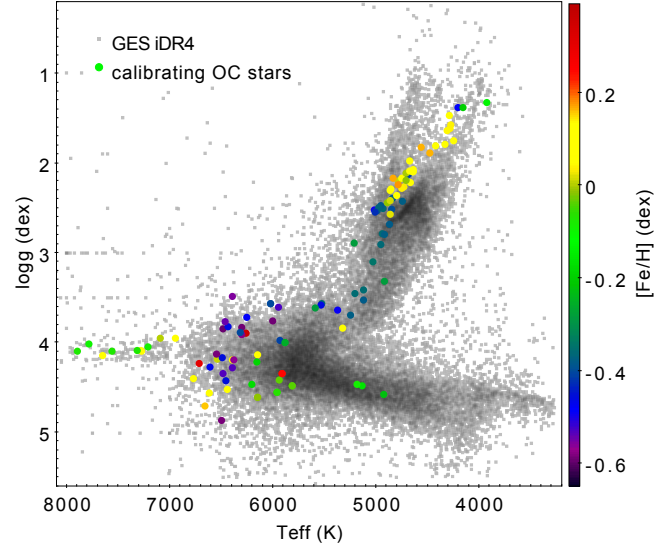


**Fig. 13.** Position on the  $T_{\text{eff}} - \log g$  plane of the stars in calibrating OCs including archival data analyzed in iDR4 (namely NGC 2243, NGC 6705, and NGC 3532) and colored according to their [Fe/H]. These stars were observed with the MW field and the OC setups. Of course, many more OC stars are observed with the OC setups alone (on the order of 20 000, see Table 1). The whole GES iDR4 sample is reported in the background as smaller gray dots.

selected stars are a subsample of those observed for scientific purposes;

- to connect stars in different evolutionary phases, that is, on the red clump and on the MS, whenever it was possible to select MS stars in a convenient magnitude range without including too many fast-rotating stars in the sample;
- to sample a range of APs to test the self-consistency of the abundance analysis, similarly to the case of GCs, by selecting stars in a range of 1–2 mag on the MS for those OCs for which a low fraction of fast rotators were present in the available magnitude ranges; in these OCs, we selected stars spanning a range of 1–2 mag.

Additionally, ESO FLAMES archival data of the relevant OCs will be included in GES, as explained above: for example, many of the stars analyzed in NGC 6705 or M 67 come from the ESO UVES archive. It is important to note that scientific OC observations can also be used by the WGs or by WG15 to homogenize the results.

## 5.3. GC selection criteria

The selection of calibrating GCs<sup>11</sup> proceeded by considering clusters that were used by other surveys such as RAVE (Steinmetz et al. 2006; Zwitter et al. 2008; Siebert et al. 2011; Lane et al. 2011), GALAH (De Silva et al. 2015; Martell 2014, priv. comm.), and APOGEE (Frinchaboy et al. 2012, 2013; Anders et al. 2014; Mészáros et al. 2013), or that were subject to numerous high-resolution studies in the past.

Another fundamental criterion was the availability of wide field ( $\approx 25'$ , the FLAMES field of view), accurate photometric data in the literature or in the archives. Unfortunately, at the time when GES started, not many public photometric catalogs were available that covered the required field of view. Therefore, we

<sup>10</sup> In any case, we did not select OCs younger than 100–200 Myr as calibrators.

<sup>11</sup> GCs are not part of the scientific targets of GES, they are only observed for calibration purposes.

**Table 7.** GES calibrating open clusters, with basic properties from Dias et al. (2002, and latest updates), and [Fe/H] metallicity from Heiter et al. (2014), except where noted.

| Cluster               | Dist<br>(pc) | $E(B - V)$<br>(mag) | Age<br>(Gyr) | [Fe/H]<br>(dex) | $\langle RV \rangle$<br>( $\text{km s}^{-1}$ ) | Status    | Notes               |
|-----------------------|--------------|---------------------|--------------|-----------------|--|-----------|---------------------|
| NGC 3532              | 492          | 0.028               | 0.30         | +0.00           | 4.33   | in iDR3   | RAVE                |
| NGC 6705 (M11)        | 1877         | 0.428               | 0.25         | +0.12           | 35.08  | in iDR3   | internal calibrator |
| NGC 2243 <sup>a</sup> | 2450         | 0.060               | 4.00         | -0.48           | 59.84  | in iDR3/4 | APOGEE              |
| Melotte 71            | 3154         | 0.113               | 0.24         | -0.27           | 0.55   | observed  | RAVE, APOGEE        |
| NGC 6253              | 1510         | 0.200               | 5.00         | +0.34           | -29.40   | observed  | very metal-rich     |
| NGC 2420              | 2480         | 0.040               | 2.00         | -0.05           | 73.57  | observed  | APOGEE              |
| NGC 2477              | 1300         | 0.240               | 0.60         | +0.07           | 7.26   | started   | RAVE, GALAH         |

**Notes.** The status column refers only to the GES calibration observations, i.e., to those OCs that were observed with the OC and MW observing setups. The last column indicates other surveys using each OC as calibrator, along with other useful annotations. <sup>(a)</sup> Distance, reddening, and age from Bragaglia & Tosi (2006).

**Table 8.** GES calibrating globular clusters, with basic properties from the Harris Galactic GC catalog (Harris 1996, 2010), except where noted.

| Cluster          | [Fe/H]<br>(dex) | $E(B - V)$<br>(mag) | $(m - M)_V$<br>(mag) | $\langle RV \rangle$<br>( $\text{km s}^{-1}$ ) | $\sigma_0$<br>( $\text{km s}^{-1}$ ) | Status    | Notes         |
|------------------|-----------------|---------------------|----------------------|--|--------------------------------------|-----------|---------------|
| NGC 1851         | -1.18           | 0.02                | 15.47                | 320.5  | 10.4                                 | in iDR1   | GALAH         |
| NGC 4372         | -2.17           | 0.39                | 15.03                | 72.3   | 3.9 <sup>a</sup>                     | in iDR1   | metal-poor    |
| NGC 5927         | -0.49           | 0.45                | 15.82                | -107.5   | 5.1 <sup>a</sup>                     | in iDR1   | metal-rich    |
| NGC 2808         | -1.14           | 0.22                | 15.59                | 101.6  | 13.4                                 | in iDR2   | well studied  |
| NGC 7078 (M 15)  | -2.37           | 0.10                | 15.39                | -107.0   | 13.5                                 | in iDR2   | APOGEE, GALAH |
| NGC 4833         | -1.85           | 0.32                | 15.08                | 200.2  | 3.9 <sup>a</sup>                     | in iDR2   | metal-poor    |
| NGC 6752         | -1.54           | 0.02                | 13.13                | -26.7  | 4.9                                  | in iDR3   | RAVE, GALAH   |
| NGC 104 (47 Tuc) | -0.72           | 0.04                | 13.37                | -18.0  | 11.0                                 | in iDR3/4 | GALAH         |
| NGC 362          | -1.26           | 0.05                | 14.83                | 223.5  | 6.4                                  | in iDR4   | GALAH         |
| NGC 1904 (M 79)  | -1.60           | 0.01                | 15.59                | 205.8  | 5.3                                  | in iDR4   | well studied  |
| NGC 7089 (M 2)   | -1.65           | 0.06                | 15.50                | -5.3   | 8.2                                  | in iDR4   | APOGEE        |
| NGC 6553         | -0.18           | 0.63                | 15.83                | -3.2   | 6.1                                  | observed  | metal-rich    |
| NGC 1261         | -1.27           | 0.01                | 16.09                | 68.2   | ...                                  | observed  | well studied  |
| NGC 6218 (M 12)  | -1.37           | 0.19                | 14.01                | -41.4  | 4.5                                  | observed  | RAVE          |

**Notes.** The status column specifies the processing cycle in which each GC was analyzed for the first time (see Sect. 2), and the last column indicates other surveys using each GC as calibrator, along with other useful annotations. <sup>(a)</sup> Radial velocity dispersion from Lardo et al. (2015).

made use of the large amount of Wide Field Imager (WFI) public GC data in the ESO archive. All relevant data were pre-reduced with IRAF and then analyzed with DAOPHOT II and ALLSTAR (Stetson 1987, 1992), and the resulting magnitudes will be published in the next public GES release. A more comprehensive set of photometric catalogs, including data from all available public archives, is being prepared by P. Stetson<sup>12</sup> and the catalogs for GES GCs will be published elsewhere. It is important to stress that for dense stellar fields like GCs, the available survey catalogs that are used to select GES targets for the MW field are not precise enough. An example of the improvement that specific crowded-field PSF-fitting techniques can bring over a standard photometric analysis was presented by An et al. (2008) for GCs in SDSS.

We thus created a sample including as many clusters as possible, selected from the other surveys calibrating samples that were visible from the southern hemisphere. We then filled the gaps in [Fe/H] with clusters with available public photometry data (from the ESO archive or from the literature). Particular care was taken to include metal-rich GCs as an interface with the OCs

(see next section) and because the majority of GES field targets are relatively metal-rich.

Twelve GCs were analyzed in iDR4, but two of them were not complete: NGC 4372 and NGC 6553. They will be fully included in subsequent releases, along with a few more GCs. A complete list of observed GCs can be found in Table 8, with the metallicity coverage illustrated in Fig. 11.

#### 5.4. Selection criteria for individual GC stars

We focused on red giants because they are generally the best-studied objects in the literature. A few subgiants and MS stars were previously observed with UVES or GIRAFFE and were included in the GES analysis cycles along with other relevant ESO archival data. For UVES, we did not observe again stars that already had good-quality UVES spectra in the archive. We did observe again with UVES a few of the stars with available GIRAFFE observations, however, to build a small sample of stars observed with both instruments for internal calibration purposes. All the other UVES targets were high-probability members based on their position in the color-magnitude diagram

<sup>12</sup> <http://www3.cadc-ccda.hia-ihp.nrc-cnrc.gc.ca/en/community/STETSON/homogeneous/>

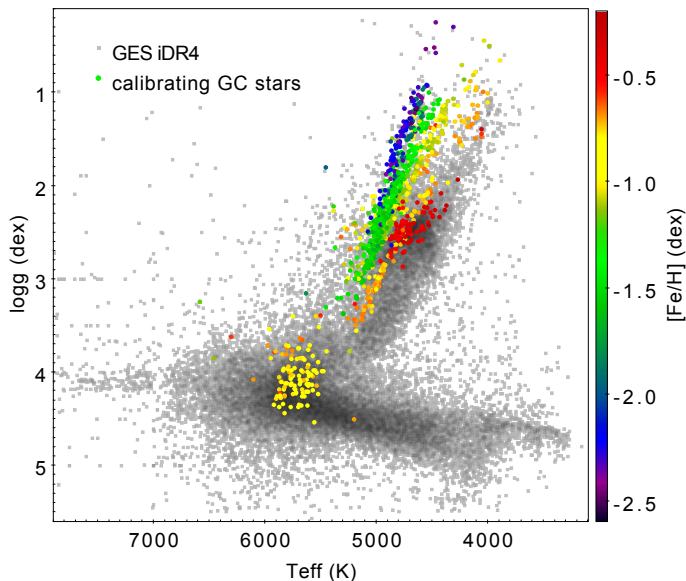


**Fig. 14.** Position on the  $T_{\text{eff}} - \log g$  plane of selected member stars in calibrating GCs, including archival data analyzed in iDR4 and colored according to their  $[\text{Fe}/\text{H}]$ . The whole GES iDR4 sample is reported in the background as smaller grey squares.

(CMD)<sup>13</sup>. Stars with companions brighter than 1% of their flux in a  $1'$  circle were excluded from observations.

For GIRAFFE, we gave highest priority to red giants with available archival observations in non-GES HR setups (see Table 1) because (i) they were in most cases analyzed and published, so that we had additional information such as RVs and chemistry to assess their membership; and (ii) a broader wavelength coverage (with more GIRAFFE setups observed) can produce a more reliable estimate of the APs and abundance ratios. Some effort was dedicated, whenever possible, to observe a few stars in common with the other spectroscopic surveys mentioned above. Whenever additional membership information was available in the literature (RVs, proper motions, metallicities), it was used to select the most probable cluster members.

Depending on the GC and on the available body of archival data, the final sample of stars analyzed in iDR4 per GC was on the order of 10–50 with UVES and 50–200 with GIRAFFE. All GES data were observed with UVES 580 and GIRAFFE HR10 and HR21. The candidates and archival data span a range of 1–3 mag along the red giant branch in each GC, which implies significant variations of APs in stars with the same  $[\text{Fe}/\text{H}]$ , thus allowing for rather precise tests on the parameters and the self-consistency of the analysis (see below). To select provisional members for this paper, we used a  $3\sigma$  cut around the median RV and  $[\text{Fe}/\text{H}]$  of the GES iDR4 recommended values, which were always fully compatible with the literature reference values reported in Table 8. The position in the theoretical  $T_{\text{eff}} - \log g$  plane of the selected members are shown in Fig. 14.

<sup>13</sup> During the first few GES runs we were forced to observe three clusters with high differential reddening because of the strict scheduling requirements: NGC 4833, NGC 5927, and NGC 4372. For these, the percentage of member stars among the selected targets was significantly lower than for the other GCs. For NGC 5927 we could rely on a published study with RVs of red clump stars (Simmerer et al. 2013), therefore in this case the majority of selected stars turned out to be members. Even if field contaminants cannot directly help with calibrations, they have an obvious scientific value for GES.

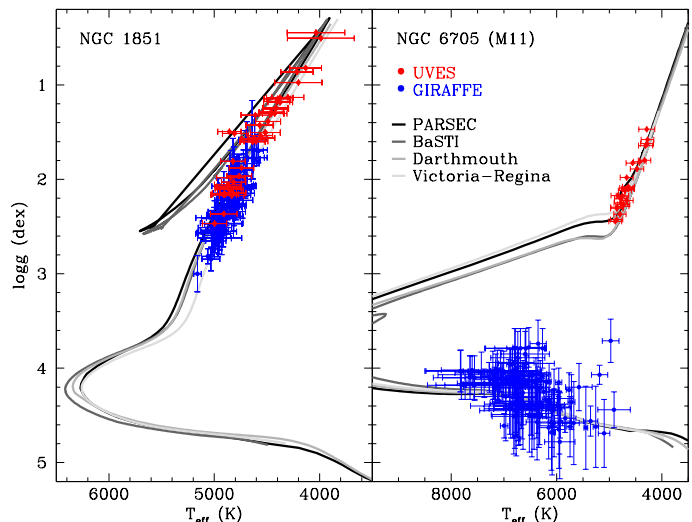


**Fig. 15.** Example of comparison with theoretical models for NGC 1851 and NGC 6705 (M 11). All stars observed in NGC 6705 are plotted, even those that are observed only with the OC setups. UVES targets are plotted in red and GIRAFFE targets in blue. Four different sets of isochrones are plotted (see text for more details) as thick lines of different colors.

### 5.5. Selected results on calibrating clusters

Clusters were used within GES past releases at many different levels to compare results obtained by different nodes, WGs, or observing setups, and to study internal trends of abundances with APs. They were useful to identify various problems that were later remedied in iDR4. Clusters were not, however, used as absolute calibrators in iDR4, but rather were used a posteriori to test the goodness of the overall homogenization process. Therefore it is interesting to compare the final iDR4 cluster recommended values with the most recent external reference values, to give an idea of the results of the whole GES homogenization procedure.

A first comparison can be made with stellar models. In Fig. 15 we show NGC 1851 and NGC 6705 as an example. A more extensive discussion and set of model comparisons will be presented in H17. We used four different sets of stellar isochrones: the PARSEC set (Bressan et al. 2012; Chen et al. 2014; Tang et al. 2014), the BaSTI set (Pietrinferni et al. 2004, 2006), the Dartmouth set (Dotter et al. 2008), and the Victoria-Regina set (VandenBerg et al. 2006). We adopted the parameters listed in Tables 7 and 8, with an age of 12.8 Gyr for NGC 1851. As can be seen, except for the small residual offset between the GIRAFFE and UVES results (see below), the GES iDR4 recommended parameters agree well with theoretical predictions within the quoted uncertainties. Considering the automated analysis, which is not tailored to obtain the best results for GCs, this is a very satisfactory result.

For a different comparison, we computed independent  $T_{\text{eff}}$  and  $\log g$  values from our photometry, described in Sect. 5.3, using the Alonso et al. (1999, 1996) calibrations for giants and dwarfs, respectively. To obtain  $T_{\text{eff}}$ , we used the  $B - V$  and  $V - K$  colors, dereddened with the  $E(B - V)$  values listed in Tables 8 and 7, and we transformed the  $K_{2\text{MASS}}$  into  $K_{\text{TCS}}$  magnitudes with the relations by Ramírez & Meléndez (2005). Similarly, we obtained  $\log g$  using bolometric corrections from the cited calibrations and fundamental relations. We assumed a fixed mass of  $0.8 M_{\odot}$  for evolved GC stars and a varying mass

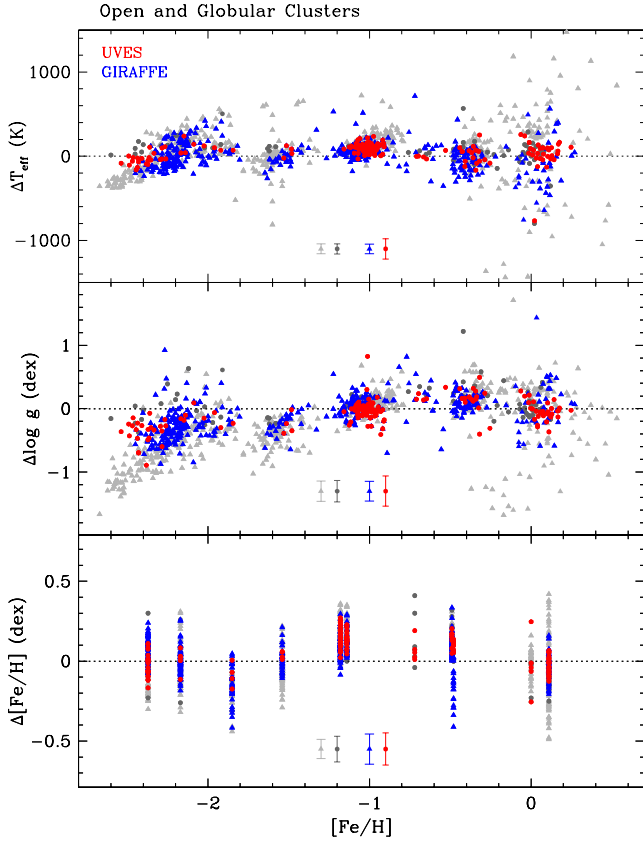


**Fig. 16.** Difference between the GES recommended APs and [Fe/H] and the photometric reference APs and literature [Fe/H] (see text for more details). The GES iDR4 results are plotted as blue triangles (for GIRAFFE) and red circles (for UVES). Grayed-out symbols represent the previous internal release (iDR2 + iDR3) corresponding values. *The top panel shows  $\Delta T_{\text{eff}}$  as a function of GES [Fe/H], the middle panel  $\Delta \log g$  as a function of GES [Fe/H], and the bottom panel  $\Delta[\text{Fe}/\text{H}]$  as a function of the literature reference [Fe/H].* The median internal errors of GES recommended values are also plotted at the center of each panel.

for OC stars at various evolutionary stages, based on the above selected isochrone sets.

The results of the comparison are presented in Fig. 16, where we also show the results obtained during the previous internal processing cycle (iDR2 + iDR3, based on data gathered in the first two years of GES observations). There clearly has been enormous improvement from the previous to the present internal data release, especially at the two extremes of the metallicity range. The causes of the improvement lie in the cyclic nature of GES data analysis and calibration, where with each cycle not only new data are added, but new procedures are introduced either to implement lessons learned in previous cycles, or to refine the quality control and data analysis. A similar analysis, based on the entire GES sample, will be presented in Randich et al. (in prep.).

The median iDR4 offsets to the reference values are always compatible with zero within the uncertainties, and the typical  $1\sigma$  spreads for UVES and GIRAFFE are compatible with the median GES errors. Of course, the selected reference parameters depend on the chosen reference cluster parameters in Tables 8 and 7, on the color-temperature calibration relations and their errors, on the accuracy and precision of the reference photometry, and so on. Had we chosen the González Hernández & Bonifacio (2009) color-temperature calibration, for example, the median  $T_{\text{eff}}$  differences reported below would have been lower by about

$\approx 60$  K. It is important to note here that the reference APs are derived with an independent method and yet the agreement is quite satisfactory, especially considering that cluster stars in GES are analyzed with the same method as field stars, that is, without profiting from the extra information on distance provided by clusters. For UVES we obtained  $\langle \Delta T_{\text{eff}} \rangle = 71 \pm 93$  K,  $\langle \Delta \log g \rangle = 0.04 \pm 0.18$  dex, and  $\langle \Delta[\text{Fe}/\text{H}] \rangle = 0.06 \pm 0.11$  dex. For GIRAFFE we obtained  $\langle \Delta T_{\text{eff}} \rangle = -49 \pm 149$  K,  $\langle \Delta \log g \rangle = -0.21 \pm 0.30$  dex, and  $\langle \Delta[\text{Fe}/\text{H}] \rangle = 0.00 \pm 0.16$  dex, where the quoted uncertainties are  $1\sigma$  spreads.

## 6. Astroseismologic constraints

The resonant frequencies of stochastically driven pulsators (such as the Sun and other FGK-type dwarfs and giants with turbulent convective envelopes) allow for precise estimates of stellar APs that are largely independent of spectroscopy (see, e.g., Miglio et al. 2013, and references therein). As an example, the surface gravity  $\log g$ , a relatively difficult quantity to measure directly from spectroscopy alone, is strongly correlated with the frequency at maximum oscillation power ( $\nu_{\text{max}}$ ):

$$\nu_{\text{max}} \propto g / \sqrt{T_{\text{eff}}}$$

(Brown 1991; Kjeldsen & Bedding 1995; Belkacem et al. 2011). Given the typical accuracy of these scaling relations and the precision of the measured  $\nu_{\text{max}}$ , the seismic estimates of  $\log g$  are likely more precise ( $\sigma_{\log g} \sim 0.05$  dex) than those derived from standard spectroscopic methods, which typically are in the range  $\sigma_{\log g} \approx 0.1$ – $0.2$  dex. We also note the weak dependence of  $\log g$  on  $T_{\text{eff}}$ : a shift in  $T_{\text{eff}}$  of  $\approx 100$  K leads to an expected variation in  $\log g$  of less than 0.01 dex, at least in the mass range covered by GES.

There is good agreement between the  $\log g$  values inferred from seismology and from classical methods for bright stars spanning a wide range of effective temperatures and evolutionary states (dwarfs, sub-giants and red giants, Morel & Miglio 2012; Morel et al. 2014). This supports the application of scaling relations in deriving weakly model-dependent  $\log g$  estimates, at least for the tested domains of metallicity and surface gravity. In the case of *Kepler*, the spectroscopic and seismic gravities have shown a good agreement, with no evidence of systematic offsets:  $\langle \log g_{\text{spec}} - \log g_{\text{seism}} \rangle = +0.08 \pm 0.07$  dex for dwarfs (Bruntt et al. 2012) and  $-0.05 \pm 0.30$  dex for giants (Thygesen et al. 2012). Fixing  $\log g$  to the seismic value in spectroscopic analysis whenever possible has become an increasingly popular technique (e.g., Huber et al. 2013). The availability of precise seismic  $\log g$  estimates for thousands of solar-like pulsators detected by CoRoT (Michel et al. 2008) and *Kepler* (Borucki et al. 2010) missions makes them valuable targets for science verification and/or calibration.

### 6.1. Asteroseismic collaborations with GES

GES observed selected targets in the LRC01 and LRA01 CoRoT fields (in the Galactic center and anticenter directions, respectively) where CoRoT has detected and characterized more than 2000 oscillating G-K red giants (Mosser et al. 2010, see also Fig. 17). More than 1500 red giants were observed with the GES field setups (Table 1) and analyzed in iDR4. A subset of a few tens of the candidates, for which the oscillation spectra have also allowed us to derive their evolutionary state (either RGB or central He-burning, Mosser et al. 2011), were observed with UVES. The GES-CoRoT collaboration will provide a set of reference

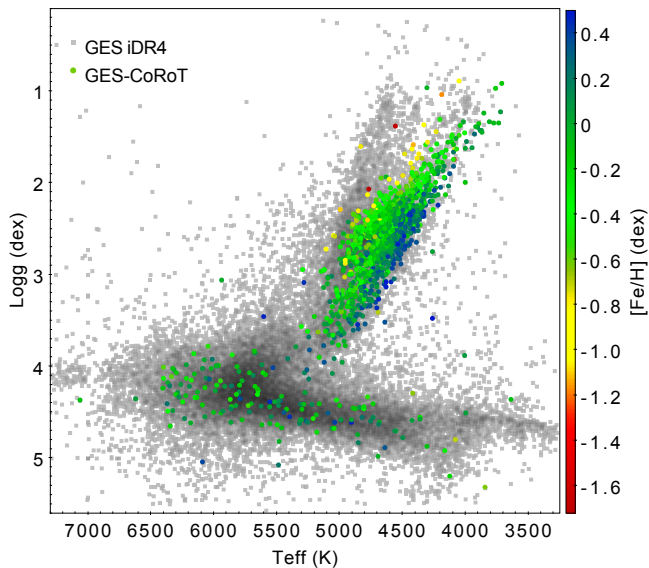


**Fig. 17.** Position in the  $T_{\text{eff}} - \log g$  plane of the GES targets in the direction of the CoRoT center and anti-center fields that were analyzed in iDR4, colored according to their  $[\text{Fe}/\text{H}]$ . The GES iDR4 analysis is not the final result because the GES-CoRoT project is still ongoing (see text for more details). The whole GES iDR4 sample is reported in the background as smaller gray squares.

parameters to compare with the GES recommended parameters, similarly to what was done by [Jofré et al. \(2014\)](#) for the benchmark stars. The final reference APs for these stars will be derived by a combined team of GES and CoRoT scientists after an iterative process: the spectroscopic  $T_{\text{eff}}$  value obtained by GES and the seismic parameter  $\nu_{\text{max}}$  will provide a first seismic  $\log g$  value, which will be held fixed in the following spectroscopic analysis by a subset of the GES abundance analysis nodes participating in the GES-CoRoT project. The new  $T_{\text{eff}}$  value will then provide a new seismic  $\log g$  estimate, and so on, until convergence (typically, no more than two iterations are needed). The results of this project will be presented elsewhere.

Similarly, thousands of solar-like oscillating giant stars have been discovered in Campaigns 1 and 3 of the K2 mission. GES observations are currently planned for a combined asteroseismic-spectroscopic analysis using individual resonant frequencies with the Birmingham asteroseismic group, allowing for far more insight into the physics of stellar interiors than what is available using simple scaling relations (e.g., [Davies et al. 2016](#)). Other spectroscopic surveys are targeting giants observed by *Kepler* and CoRoT for similar purposes, so that a large sample of overlapping spectroscopic observations is expected (see also [Fig. 18](#)), allowing for future survey intercalibrations. More details on the target selection strategy, data analysis, and use of these calibrators for the intercalibration with other surveys can be found in [Gilmore et al. \(in prep.\)](#).

## 7. Discussion and conclusions

The GES calibration and data analysis strategy is designed to ensure the internal consistency and the overall reliability of its results with respect to literature or reference values. The abundance analysis process in GES is complex, resulting from observations of different objects with different instrumental setups, and analyzed by several abundance analysis nodes, using virtually all of the existing most recent techniques. While this is one of the main strengths of the GES data analysis, it requires

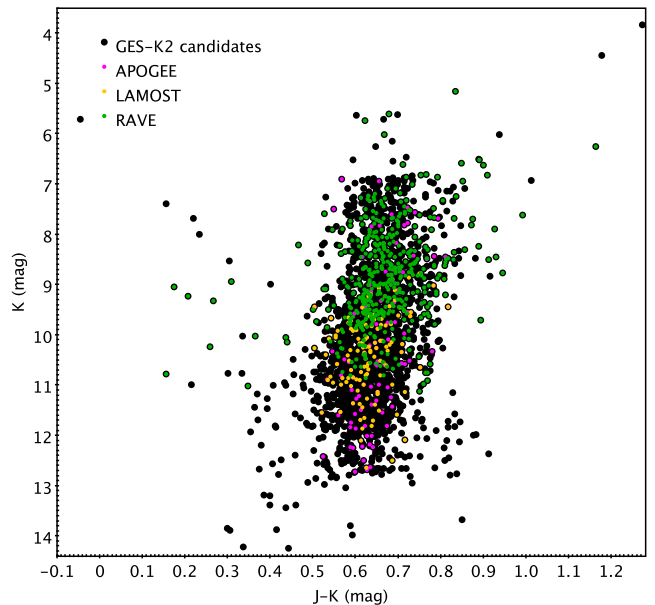


**Fig. 18.** *Kepler* red giants in the K2 C1 and C3 fields that were selected as candidates for GES observations (large black circles). Stars previously observed by other surveys are highlighted in different colors (APOGEE in magenta, LAMOST in yellow, and RAVE in green).

particular attention in the process of data homogenization, which produces the GES recommended RVs, APs, and chemical abundance ratios.

Different classes of calibrating objects were selected, with the main goals of covering the different observational setups, the AP space covered by the GES scientific targets, and the variety of methods used to analyze them. In particular, we selected a sample of 31 RV standards from the *Gaia* RV standards catalog ([Soubiran et al. 2013](#)); a pool of star clusters, GCs and OCs, either used as calibrators by other major ongoing surveys or well studied in the literature, of which 21 were observed to date; a list of FGK benchmark stars in common with the *Gaia* list of benchmarks ([Heiter et al. 2015b](#)) was observed, complemented by cooler M benchmarks and OBA candidate benchmark stars; and a list of thousands of targets in common with those of the two main asteroseismic space missions, CoRoT and *Kepler*, was also observed. In a few cases the calibration planning of GES and its requirements have spawned calibration projects like the *Gaia* benchmarks spectroscopic project ([Blanco-Cuaresma et al. 2014](#); [Jofré et al. 2014, 2015](#); [Hawkins et al. 2016](#)) or the GES-CoRoT collaboration, which will prove useful for many other projects and surveys.

The complex GES calibration and homogenization procedures as described in [Smiljanic et al. \(2014\)](#), [Lanzafame et al. \(2015\)](#), and H17 are applied at different levels of the data processing (node, WG, and survey-wide), and they are applied to all the GES targets (field stars, OC scientific targets, and calibrators). Therefore, it is particularly instructive to examine the outcome of the whole calibration process on the calibrating objects themselves. We presented a few examples of the comparisons that are routinely performed in GES. In particular, we showed how the cyclic processing leads to significant improvement from cycle to cycle. We also quantitatively showed that the agreement between GES iDR4 recommended values and reference values for the calibrating objects are very satisfactory. The average offsets and spreads are generally compatible with the GES measurement errors, proving that the performance goals set by [Gilmore et al. \(2012\)](#) and [Randich et al. \(2013\)](#) are being met.

**Acknowledgements.** Based on data products from observations made with ESO Telescopes at the La Silla Paranal Observatory under program ID 188.B-3002 and 193.B-0936. These data products have been processed by the Cambridge Astronomy Survey Unit (CASU) at the Institute of Astronomy, University of Cambridge, and by the FLAMES/UVES reduction team at INAF-Osservatorio Astrofisico di Arcetri. These data have been obtained from the *Gaia*-ESO Survey Data Archive, prepared and hosted by the Wide Field Astronomy Unit, Institute for Astronomy, University of Edinburgh, which is funded by the UK Science and Technology Facilities Council. This work was partly supported by the European Union FP7 program through ERC grant number 320360 and by the Leverhulme Trust through grant RPG-2012-541. We acknowledge the support from INAF and Ministero dell’Istruzione, dell’Università e della Ricerca (MIUR) in the form of the grant “Premiale VLT 2012”. The results presented here benefit from discussions held during the *Gaia*-ESO workshops and conferences supported by the ESF (European Science Foundation) through the GREAT Research Network Programme. S.F. and T.B. acknowledge the support from the New Milky Way project funded by a grant from the Knut and Alice Wallenberg foundation. C.L. gratefully acknowledges financial support from the European Research Council (ERC-CoG-646928, Multi-Pop, PI: N. Bastian). U.H. and A.J.K. acknowledge support from the Swedish National Space Board (Rymdstyrelsen). The research of A.L. has been subsidized by the Belgian Federal Science Policy Office under contract No. BR/143/A2/BRASS. R.S. acknowledges support by the National Science Center of Poland through grant 2014/15/B/ST9/03981. C.A.P. is thankful for support from the Spanish Ministry of Economy and Competitiveness (MINECO) through grant AYA2014-56359-P. J.M. acknowledges support from the ERC Consolidator Grant funding scheme (project STARKEY, G.A. No. 615604). T.M. acknowledges financial support from Belspo for contract PRODEX *Gaia*-DPAC. S.G.S. acknowledges the support by Fundação para a Ciência e Tecnologia (FCT) through national funds and a research grant (project ref. UID/FIS/04434/2013, and PTDC/FIS-AST/7073/2014). S.G.S. also acknowledge the support from FCT through Investigador FCT contract of reference IF/00028/2014 and POPH/FSE (EC) by FEDER funding through the program “Programa Operacional de Factores de Competitividade – COMPETE”. L.S. acknowledges support by the Ministry of Economy, Development, and Tourism’s Millennium Science Initiative through grant IC120009, awarded to The Millennium Institute of Astrophysics (MAS). M.Z. acknowledges support by the Ministry of Economy, Development, and Tourism’s Millennium Science Initiative through grant IC120009, awarded to The Millennium Institute of Astrophysics (MAS), by Fondecyt Regular 1150345 and by the BASAL CATA PFB-06. E.J.A. and M.T.C. acknowledge the financial support from the Spanish Ministerio de Economía y Competitividad, through grant AYA2013-40611-P. S.Z. acknowledge the support from the INAF grant “PRIN INAF 2014”, “Star won’t tell their ages to *Gaia*, Galactic Archaeology with wide-area asteroseismic”. This research has made use of the WEBDA database, operated at the Department of Theoretical Physics and Astrophysics of the Masaryk University; of the TOPCAT catalogue handling and plotting tool (Taylor 2005); of the Simbad database and the VizieR catalog access tool, CDS, Strasbourg, France (Ochsenbein et al. 2000); and of NASA’s Astrophysics Data System.

## References

- Alonso, A., Arribas, S., & Martínez-Roger, C. 1996, *A&A*, 313, 873
- Alonso, A., Arribas, S., & Martínez-Roger, C. 1999, *A&AS*, 140, 261
- An, D., Johnson, J. A., Clem, J. L., et al. 2008, *ApJS*, 179, 326
- Anders, F., Chiappini, C., Santiago, B. X., et al. 2014, *A&A*, 564, A115
- Bailer-Jones, C. A. L., Andrae, R., Arcay, B., et al. 2013, *A&A*, 559, A74
- Balcells, M., Benn, C. R., Carter, D., et al. 2010, *Proc. SPIE*, 7735, 77357G
- Ballester, P., Modigliani, A., Boitquin, O., et al. 2000, *The Messenger*, 101, 31
- Barbá, R. H., Gamén, R., Arias, J. I., et al. 2010, *Rev. Mex. Astron. Astrofis. Conf. Ser.*, 38, 30
- Barbá, R., Gamén, R., Arias, J. I., et al. 2014, *Rev. Mex. Astron. Astrofis. Conf. Ser.*, 44, 148
- Barden, S. C., Jones, D. J., Barnes, S. I., et al. 2010, *Proc. SPIE*, 7735, 773509
- Belkacem, K., Goupil, M. J., Dupret, M. A., et al. 2011, *A&A*, 530, A142
- Bensby, T., Feltzing, S., & Oey, M. S. 2014, *A&A*, 562, A71
- Bertaux, J. L., Lallement, R., Ferron, S., Boonne, C., & Bodichon, R. 2014, *A&A*, 564, A46
- Blanco-Cuaresma, S., Soubiran, C., Jofré, P., & Heiter, U. 2014, *A&A*, 566, A98
- Bland-Hawthorn, J., Krumholz, M. R., & Freeman, K. 2010, *ApJ*, 713, 166
- Boyajian, T. S., von Braun, K., van Belle, G., et al. 2012, *ApJ*, 757, 112
- Borucki, W. J., Koch, D., Basri, G., et al. 2010, *Science*, 327, 977
- Bragaglia, A., & Tosi, M. 2006, *AJ*, 131, 1544
- Bressan, A., Marigo, P., Girardi, L., et al. 2012, *MNRAS*, 427, 127
- Brown, T. M. 1991, *ApJ*, 371, 396
- Bruntt, H., Basu, S., Smalley, B., et al. 2012, *MNRAS*, 423, 122
- Burkhardt, C., & Coupry, M. F. 1989, *A&A*, 220, 197
- Chen, Y., Girardi, L., Bressan, A., et al. 2014, *MNRAS*, 444, 2525
- Chubak, C., Marcy, G., Fischer, D. A., et al. 2012, [arXiv e-prints [arXiv:1207.6212]]
- Dafon, S., & Cunha, K. 2004, *ApJ*, 617, 1115
- Davies, G. R., Silva Aguirre, V., Bedding, T. R., et al. 2016, *MNRAS*, 456, 2183
- de Bruijne, J. H. J. 2012, *Ap&SS*, 341, 31
- de Jong, R. S., Barden, S., Bellido-Tirado, O., et al. 2014, *Proc. SPIE*, 9147, 91470M
- de Laverny, P., Recio-Blanco, A., Worley, C. C., & Plez, B. 2012, *A&A*, 544, A126
- Demory, B.-O., Ségransan, D., Forveille, T., et al. 2009, *A&A*, 505, 205
- De Pascale, M., Worley, C. C., de Laverny, P., et al. 2014, *A&A*, 570, A68
- De Silva, G. M., Freeman, K. C., Bland-Hawthorn, J., et al. 2015, *MNRAS*, 449, 2604
- Dias, W. S., Alessi, B. S., Moitinho, A., & Lépine, J. R. D. 2002, *A&A*, 389, 871
- Donati, P., Cantat Gaudin, T., Bragaglia, A., et al. 2014, *A&A*, 561, A94
- Dotter, A., Chaboyer, B., Jevremović, D., et al. 2008, *ApJS*, 178, 89
- Freeman, K., & Bland-Hawthorn, J. 2002, *ARA&A*, 40, 487
- Frinchaboy, P. M., Allende Prieto, C., Beers, T. C., et al. 2012, *AAS Meeting Abstracts*, 219, 428.04
- Frinchaboy, P. M., Thompson, B., Jackson, K. M., et al. 2013, *ApJ*, 777, L1
- Gaia* Collaboration (Prusti, T., et al.) 2016a, *A&A*, 595, A1
- Gaia* Collaboration (Brown, A. G. A., et al.) 2016b, *A&A*, 595, A2
- Gilmore, G., Randich, S., Asplund, M., et al. 2012, *The Messenger*, 147, 25
- González Hernández, J. I., & Bonifacio, P. 2009, *A&A*, 497, 497
- Gratton, R. G., Carretta, E., & Bragaglia, A. 2012, *A&ARv*, 20, 50
- Gustafsson, B., Edvardsson, B., Eriksson, K., et al. 2008, *A&A*, 486, 951
- Harris, W. E. 1996, *AJ*, 112, 1487
- Harris, W. E. 2010, [arXiv e-prints [arXiv:1012.3224]]
- Hawkins, K., Jofré, P., Heiter, U., et al. 2016, *A&A*, 592, A70
- Heiter, U., Soubiran, C., Netopil, M., & Paurzen, E. 2014, *A&A*, 561, A93
- Heiter, U., Lind, K., Asplund, M., et al. 2015a, *Phys. Scr.*, 90, 054010
- Heiter, U., Jofré, P., Gustafsson, B., et al. 2015b, *A&A*, 582, A49
- Huber, D., Chaplin, W. J., Christensen-Dalsgaard, J., et al. 2013, *ApJ*, 767, 127
- Hubrig, S., Briquet, M., Morel, T., et al. 2008, *A&A*, 488, 287
- Irrgang, A., Przybilla, N., Heber, U., et al. 2014, *A&A*, 565, A63
- Jackson, R. J., Jeffries, R. D., Lewis, J., et al. 2015, *A&A*, 580, A75
- Jeffries, R. D., Maxted, P. F. L., Oliveira, J. M., & Naylor, T. 2006, *MNRAS*, 371, L6
- Jeffries, R. D., Jackson, R. J., Cottaar, M., et al. 2014, *A&A*, 563, A94
- Jofré, P., Heiter, U., Soubiran, C., et al. 2014, *A&A*, 564, A133
- Jofré, P., Heiter, U., Soubiran, C., et al. 2015, *A&A*, 582, A81
- Kjeldsen, H., & Bedding, T. R. 1995, *A&A*, 293, 87
- Koposov, S. E., Gilmore, G., Walker, M. G., et al. 2011, *ApJ*, 736, 146
- Kordopatis, G., Gilmore, G., Steinmetz, M., et al. 2013, *AJ*, 146, 134
- Lane, R. R., Kiss, L. L., Lewis, G. F., et al. 2011, *A&A*, 530, A31
- Lanzafame, A. C., Frasca, A., Damiani, F., et al. 2015, *A&A*, 576, A80
- Lardo, C., Pancino, E., Bellazzini, M., et al. 2015, *A&A*, 573, A115
- Lebzelter, T., Seifahrt, A., Utenthaler, S., et al. 2012, *A&A*, 539, A109
- Lefever, K., Puls, J., Morel, T., et al. 2010, *A&A*, 515, A74
- Lindgren, L., & Perryman, M. A. C. 1996, *A&AS*, 116, 579
- Lindgren, S., Heiter, U., & Seifahrt, A. 2016, *A&A*, 586, A100
- Maíz Apellániz, J., Alfaro, E. J., Arias, J. I., et al. 2015, Highlights of Spanish Astrophysics VIII, 603
- Majewski, S. R., Schiavon, R. P., Frinchaboy, P. M., et al. 2016, *Astron. Nachr.*, 337, 863
- Markova, N., Puls, J., Simón-Díaz, S., et al. 2014, *A&A*, 562, A37
- Martins, F., Escolano, C., Wade, G. A., et al. 2012, *A&A*, 538, A29
- Martins, F., Hervé, A., Bouret, J.-C., et al. 2015, *A&A*, 575, A34
- Mészáros, S., Holtzman, J., García Pérez, A. E., et al. 2013, *AJ*, 146, 133
- Michel, E., Baglin, A., Auvergne, M., et al. 2008, *Science*, 322, 558
- Miglio, A., Chiappini, C., Morel, T., et al. 2013, *EPJ Web Conf.*, 43, 03004
- Mignard, F. 2005, *Astrometry in the Age of the Next Generation of Large Telescopes, ASP Conf. Ser.*, 338, 15
- Mokiem, M. R., de Koter, A., Puls, J., et al. 2005, *A&A*, 441, 711
- Morel, T., & Butler, K. 2008, *A&A*, 487, 307
- Morel, T., & Miglio, A. 2012, *MNRAS*, 419, L34
- Morel, T., Miglio, A., Lagarde, N., et al. 2014, *A&A*, 564, A119
- Mosser, B., Belkacem, K., Goupil, M.-J., et al. 2010, *A&A*, 517, A22
- Mosser, B., Barban, C., Montalbán, J., et al. 2011, *A&A*, 532, A86
- Neves, V., Bonfils, X., Santos, N. C., et al. 2014, *A&A*, 568, A121
- Newberg, H. J., Carlin, J. L., Chen, L., et al. 2012, *Galactic Archaeology: Near-Field Cosmology and the Formation of the Milky Way*, 458, 405
- Nieva, M.-F., & Przybilla, N. 2012, *A&A*, 539, A143
- Nieva, M.-F., & Simón-Díaz, S. 2011, *A&A*, 532, A2
- Ochsenbein, F., Bauer, P., & Marcout, J. 2000, *A&AS*, 143, 23
- Önehag, A., Heiter, U., Gustafsson, B., et al. 2012, *A&A*, 542, A33

- Pasquini, L., Avila, G., Allaert, E., et al. 2000, *Proc. SPIE*, **4008**, 129
- Pietrinferni, A., Cassisi, S., Salaris, M., & Castelli, F. 2004, *ApJ*, **612**, 168
- Pietrinferni, A., Cassisi, S., Salaris, M., & Castelli, F. 2006, *ApJ*, **642**, 797
- Przybilla, N., Nieva, M.-F., & Butler, K. 2011, *J. Phys. Conf. Ser.*, **328**, 012015
- Ramírez, I., & Allende Prieto, C. 2011, *ApJ*, **743**, 135
- Ramírez, I., & Meléndez, J. 2005, *ApJ*, **626**, 446
- Randich, S., Gilmore, G., & Gaia-ESO Consortium 2013, *The Messenger*, **154**, 47
- Repolust, T., Puls, J., & Herrero, A. 2004, *A&A*, **415**, 349
- Rojas-Ayala, B., Covey, K. R., Muirhead, P. S., & Lloyd, J. P. 2012, *ApJ*, **748**, 93
- Sacco, G. G., Morbidelli, L., Franciosini, E., et al. 2014, *A&A*, **565**, A113
- Siebert, A., Williams, M. E. K., Siviero, A., et al. 2011, *AJ*, **141**, 187
- Simmerer, J., Feltzing, S., & Primas, F. 2013, *A&A*, **556**, A58
- Simón-Díaz, S., Herrero, A., Esteban, C., & Najarro, F. 2006, *A&A*, **448**, 351
- Simón-Díaz, S., Castro, N., García, M., Herrero, A., & Markova, N. 2011a, *Bull. Soc. Roy. Sci. Liège*, **80**, 514
- Simón-Díaz, S., García, M., Herrero, A., Maíz Apellániz, J., & Negueruela, I. 2011b, *Stellar Clusters & Associations: A RIA Workshop on Gaia*, 255
- Simón-Díaz, S., Negueruela, I., Maíz Apellániz, J., et al. 2015, *Highlights of Spanish Astrophysics VIII*, 576
- Smiljanic, R., Korn, A. J., Bergemann, M., et al. 2014, *A&A*, **570**, A122
- Smith, K. C., & Dworetsky, M. M. 1993, *A&A*, **274**, 335
- Soubiran, C., Jasniewicz, G., Chemin, L., et al. 2013, *A&A*, **552**, A64
- Sousa, S. G., Santos, N. C., Adibekyan, V., et al. 2014, *A&A*, **561**, A21
- Steinmetz, M., Zwitter, T., Siebert, A., et al. 2006, *AJ*, **132**, 1645
- Stetson, P. B. 1987, *PASP*, **99**, 191
- Stetson, P. B. 1992, *Astronomical Data Analysis Software and Systems I*, **25**, 297
- Taylor, M. B. 2005, *Astronomical Data Analysis Software and Systems XIV*, **347**, 29
- Tang, J., Bressan, A., Rosenfield, P., et al. 2014, *MNRAS*, **445**, 4287
- Thygesen, A. O., Frandsen, S., Bruntt, H., et al. 2012, *A&A*, **543**, A160
- VandenBerg, D. A., Bergbusch, P. A., & Dowler, P. D. 2006, *ApJS*, **162**, 375
- von Braun, K., Boyajian, T. S., Kane, S. R., et al. 2011, *ApJ*, **729**, L26
- von Braun, K., Boyajian, T. S., Kane, S. R., et al. 2012, *ApJ*, **753**, 171
- Walborn, N. R., & Fitzpatrick, E. L. 1990, *PASP*, **102**, 379
- Worley, C. C., de Laverny, P., Recio-Blanco, A., et al. 2012, *A&A*, **542**, A48
- Zwitter, T., Siebert, A., Munari, U., et al. 2008, *AJ*, **136**, 421
- <sup>11</sup> Institute of Astronomy, University of Cambridge, Madingley Road, Cambridge CB3 0HA, UK
- <sup>12</sup> Royal Observatory of Belgium, Ringlaan 3, 1180 Brussels, Belgium
- <sup>13</sup> Institut d'Astrophysique et de Géophysique, Université de Liège, Allée du 6 Août, Bât. B5c, 4000 Liège, Belgium
- <sup>14</sup> Instituto de Astrofísica de Canarias, 38200 La Laguna, Tenerife, Spain
- <sup>15</sup> Departamento de Astrofísica, Universidad de La Laguna, 38205 La Laguna, Tenerife, Spain
- <sup>16</sup> Laboratoire d'astrophysique de Bordeaux, Univ. Bordeaux, CNRS, B18N, allée Geoffroy Saint-Hilaire, 33615 Pessac, France
- <sup>17</sup> Dipartimento di Fisica e Astronomia, Università di Padova, Vicolo dell'Osservatorio 2, 35122 Padova, Italy
- <sup>18</sup> Leibniz Institute für Astrophysics (AIP), An der Sternwarte 16, 14482 Potsdam, Germany
- <sup>19</sup> Observatoire de Genève, Université de Genève, 1290 Versoix, Switzerland
- <sup>20</sup> Núcleo de Astronomía, Facultad de Ingeniería, Universidad Diego Portales, Av. Ejercito 441, Santiago, Chile
- <sup>21</sup> GEPI, Observatoire de Paris, PSL Research University, CNRS, Univ. Paris Diderot, Sorbonne Paris Cité, 5 place Jules Janssen, 92190 Meudon, France
- <sup>22</sup> Lund Observatory, Department of Astronomy and Theoretical Physics, Box 43, 221 00 Lund, Sweden
- <sup>23</sup> Research School of Astronomy & Astrophysics, Australian National University, Cotter Road, Weston Creek, ACT 2611, Australia
- <sup>24</sup> Centre for Astrophysics Research, STRI, University of Hertfordshire, College Lane Campus, Hatfield AL10 9AB, UK
- <sup>25</sup> Astrophysics Group, Research Institute for the Environment, Physical Sciences and Applied Mathematics, Keele University, Keele, Staffordshire ST5 5BG, UK
- <sup>26</sup> INAF-Osservatorio Astronomico di Palermo, Piazza del Parlamento 1, 90134 Palermo, Italy
- <sup>27</sup> INAF-Padova Observatory, Vicolo dell'Osservatorio 5, 35122 Padova, Italy
- <sup>28</sup> Instituto de Astrofísica de Andalucía-CSIC, Apdo. 3004, 18080 Granada, Spain
- <sup>29</sup> Institute of Astronomy, University of Edinburgh, Blackford Hill, Edinburgh EH9 3HJ, UK
- <sup>30</sup> Dipartimento di Fisica e Astronomia, Sezione Astrofisica, Università di Catania, via S. Sofia 78, 95123 Catania, Italy
- <sup>31</sup> Nicolaus Copernicus Astronomical Center, Polish Academy of Sciences, ul. Bartycka 18, 00-716 Warsaw, Poland
- <sup>32</sup> Institut d'Astronomie et d'Astrophysique, Université libre de Brussels, Boulevard du Triomphe, 1050 Brussels, Belgium
- <sup>33</sup> Instituto de Física y Astronomía, Universidad de Valparaíso, Chile
- <sup>34</sup> INAF-Osservatorio Astrofisico di Catania, via S. Sofia 78, 95123 Catania, Italy
- <sup>35</sup> Departamento de Ciencias Físicas, Universidad Andres Bello, Republica 220, Santiago, Chile
- <sup>36</sup> European Southern Observatory, Alonso de Cordova 3107 Vitacura, Santiago de Chile, Chile
- <sup>37</sup> Instituto de Astrofísica e Ciências do Espaço, Universidade do Porto, CAUP, rua das Estrelas, 4150-762 Porto, Portugal
- <sup>38</sup> Physics Department, Lancaster University, Lancaster LA1 4YB, UK
- <sup>39</sup> UPJV, Université de Picardie Jules Verne, 33 rue St Leu, 80080 Amiens, France
- <sup>1</sup> INAF-Osservatorio Astrofisico di Arcetri, Largo E. Fermi 5, 50125 Firenze, Italy  
e-mail: pancino@arcetri.inaf.it
- <sup>2</sup> ASI Science Data Center, via del Politecnico s/n, 00133 Roma, Italy
- <sup>3</sup> Astrophysics Research Institute, Liverpool John Moores University, 146 Brownlow Hill, Liverpool L3 5RF, UK
- <sup>4</sup> INAF-Osservatorio Astronomico di Bologna, via Ranzani 1, 40127 Bologna, Italy
- <sup>5</sup> INAF-Osservatorio Astronomico di Roma, via Frascati 33, 00040 Monte Porzio Catone, Roma, Italy
- <sup>6</sup> Space Telescope Science Institute, 3700 San Martin Drive, Baltimore, MD 21218, US
- <sup>7</sup> Instituto de Astrofísica, Pontificia Universidad Católica de Chile, Av. Vicuña Mackenna 4860, 782-0436 Macul, Santiago, Chile
- <sup>8</sup> Millennium Institute of Astrophysics, Av. Vicuña Mackenna 4860, 782-0436 Macul, Santiago, Chile
- <sup>9</sup> Dipartimento di Fisica e Astronomia, Alma Mater Studiorum, Università di Bologna, Viale Berti Pichat 6/2, 40127 Bologna, Italy
- <sup>10</sup> Department of Physics and Astronomy, Uppsala University, Box 516, 751 20 Uppsala, Sweden